Chemistry and Physics of Lipids, 32 (1983) 179–250
Elsevier Scientific Publishers Ireland Ltd.

FLUORESCENCE DEPOLARIZATION IN LIQUID CRYSTALS AND MEMBRANE BILAYERS

CLAUDIO ZANNONI[a], ALBERTO ARCIONI[b] and PAOLO CAVATORTA[c]

[a] *Istituto di Chimica Organica,* [b] *Istituto di Chimica Fisica, Universitá, Viale Risorgimento, 4, 40136 Bologna and* [c] *Istituto di Fisica, Facoltá di Scienze, Universitá, Parma (Italy)*

Received July 15th, 1982

The paper introduces in a systematic way the concepts of order parameters and correlation functions needed for a description of orientational ordering in a liquid crystal or a membrane bilayer. The strong collision and the diffusion model for reorientation are examined in some detail. After discussing the main characteristics of the very popular probes 1,6 diphenylhexatriene (DPH) and perylene the theory of rotational depolarization of fluorescence for a probe in an ordered phase is introduced. Time-dependent and steady state experiments in monodomains are discussed together with their angular dependence. Attention is then focussed on membrane vesicles. The theory for fluorescence depolarization is presented for probes with any orientation of the transition moments with a view to investigating the feasibility of using a certain probe to extract information on ordering and dynamics. Applications of the fluorescence depolarization technique to model and biological membranes are briefly reviewed. An appendix introducing irreducible tensors and Wigner rotation matrices properties is provided in order to keep the paper reasonably self-contained.

Keywords: membranes; fluorescence depolarization; liquid crystals; probes; order.

1. Introduction

Time-dependent fluorescence depolarization represents a useful tool for the investigation of molecular motions in liquids [1–3], in liquid crystals [4–6] and in biological systems [7–19]. Although the basis for a theoretical understanding of the reorientational depolarization phenomenon dates back to Perrin's work [1] nearly 50 years ago, the great development of the fluorescence depolarization (FD) technique can be ascribed to the advent of nanosecond [7] and, more recently, picosecond pulse [3] techniques. In these experimental methods a short burst of plane polarized light of suitable wavelength is used to promote fluorescent probe molecules in solution to some excited level. The polarization of the fluorescent emission from the probe is then measured as a function of time. A common, convenient way of defining the polarization characteristic of the emitted radiation in an isotro-

pic system is through the ratio

$$r(t) = (I_{\parallel}(t) - I_{\perp}(t))/(I_{\parallel}(t) + 2I_{\perp}(t))$$

where $I_{\parallel}(t)$ and $I_{\perp}(t)$ are fluorescence intensities parallel and perpendicular to the direction of polarization of the exciting light. It is easy to see that this polarization decay may contain information on the molecular motion. Let us assume that the only two relevant processes taking place in the experiment time scale are the decay of fluorescence and the reorientation of the molecule. What is actually observed in the experiment depends on the relative time scales τ_F and τ_R of the fluorescence and reorientation process [4]. Thus if $\tau_F \ll \tau_R$, the molecule emits before the non-equilibrium distribution of excited molecules created by the flash has had time to relax to equilibrium. In this case a constant value of the polarization ratio, $r(0)$, will be observed. The opposite situation arises if $\tau_F \gg \tau_R$. In this limit the initial non-equilibrium orientational distribution will have completely relaxed to equilibrium before fluorescence effectively takes place. Only a limiting value $r(\infty)$ is observed. In ordinary isotropic liquids every orientation of the probe is, in principle, equally probable and the initial polarization of the radiation will be eventually lost completely i.e. $r(\infty) = 0$. The situation is quite different in ordered fluid systems (mesophases) such as liquid crystals or membrane bilayers, since there the orientational distribution is intrinsically anisotropic. Therefore in an aligned liquid crystal we do not expect even the long time ratio limit $r(\infty)$ to go to zero but to depend on the orientational order for the probe. In the other limiting situation, when the fluorescence decays before the molecule has effectively reoriented, a value of $r(0)$ dependent on the degree of orientational alignment will be obtained [4].

For what concerns the FD investigation of membranes, one important point to notice is that the bilayer interior is very similar to a liquid crystal at least in the sense that there exists orientational order, with molecules tending to be parallel to a preferred orientation called the director. Under normal circumstances this preferred direction should be parallel to the bilayer normal. In a real experimental situation an ideal mono-domain bilayer may be rather difficult to obtain and the sample will contain a distribution of bilayers and therefore of directors. If we deal with vesicles, as is often the case, this distribution of directors will be spherical and the sample macroscopically unoriented. Until a few years ago, this led to some misinterpretation in the literature with the application to the analysis of FD data in membranes of the classical Perrin type theories developed for truly isotropic systems. This theory predicts in particular that $r(\infty)$ should be zero, as well as attributing the unobserved decay to this zero value to a large viscosity in the bilayer. This is not necessarily the case. The direct application of Perrin's theory to vesicles neglects in fact the all important local

order in the bilayer. Since FD is a molecular technique, where the probe senses its local environment, it turns out to be useful and indeed often necessary to apply theoretical methods employed in the description of liquid crystals to properly describe fluorescence polarization decay in membranes. Thus, in a sense, liquid crystals serve as useful models for studying vesicles, while these in turn serve as models for real membranes. This point of view has shown its validity and potentiality in various techniques, ranging from Nuclear Magnetic Resonance (NMR) [20] to Electron Spin Resonance (ESR) [21, 22] to FD itself [19]. Part of the problem in applying the liquid crystal concepts to the membrane field seems to be a communication gap. This is further complicated by the fact that many terms are common to the membrane and the liquid crystal field, while their significance is more or less profoundly different. Thus terms like order, fluidity, etc. are used in both areas. Actually it seems that certain terms have been often used as synonymous in some membrane work, e.g. rigidity and order, while a more careful analysis shows them to be two quite different types of property. The liquid crystal approach to membrane bilayers should help in clarifying and rendering more precise the use of these concepts. In view of this, the plan of the present paper is as follows. First we shall discuss some general concepts needed for the description of a system with orientational order [23]. We shall then describe the theory of FD in ordered and locally ordered systems. We shall limit ourselves to considering time dependent and steady state experiments where the depolarizing mechanism is reorientational and discuss briefly how this limit can be achieved in a real experimental situation. A few popular fluorescent probes [24] such as 1,6-diphenylhexatriene (DPH) and perylene will be discussed in some detail, together with a brief review of their applications in the membrane field.

This approach will involve a little bit of mathematics. We shall try to keep this to a minimum, but after all we think that its introduction requires little in the way of apologies. Experimental techniques become more sophisticated and powerful and, from the outside, more complicated all the time. It is clear that paralleling an increase in sophistication of the experimental methods there is an attendant wealth of information produced. It is not surprising that this in turn will increase the complexity of the theoretical treatment required to interpret the data properly. It should be pointed out, however, that using a complicated piece of equipment does not necessarily mean knowing every detail of its inside workings. Rather it entails being familiar with the general principles of its functioning, knowing how to operate it properly and when that particular instrument should be used instead of another one. Similarly much of the theory presented is implemented as a set of one or more computer programs which can be largely used as a black box.

From what we have just said it should be clear that we do not aim to

provide a comprehensive review of all that has been done using fluorescence depolarization in the membrane field. We shall also not discuss in detail arguments such as the perturbation of the membrane bilayer produced by probes etc. since these points have been taken up in a number of recent papers and reviews [24]. Rather we shall try to provide a coherent account of the physics necessary to plan a FD experiment and to analyze the data produced by such an experiment, together with a somewhat selected review of applications.

2. The description of ordered systems

2.1. Static properties

A brief introduction to the theoretical description of orientationally ordered systems is necessary to establish notation and to discuss the parameters we may then try to measure using FD. We shall concentrate in particular on a systematic introduction of the concepts of orientational order, and later on, of correlation times. To start with we consider here the description of a system as simple as possible, i.e. of a classical, rigid, cylindrically symmetric probe particle with centre of mass at position $\boldsymbol{r}$ and orientation Ω embedded in an ordered fluid. The assumption of cylindrical symmetry means that only two angles suffice to specify the molecular orientation (cf. Fig. 2.1). Notice, however, that real molecules are often neither cylindrically symmetric nor rigid, for they can have e.g. flexible chains or rings that can rotate with respect to each other. We shall therefore have to expect that, beyond a certain level of sophistication, features like deviation from cylindrical symmetry and flexibility will have to be taken into

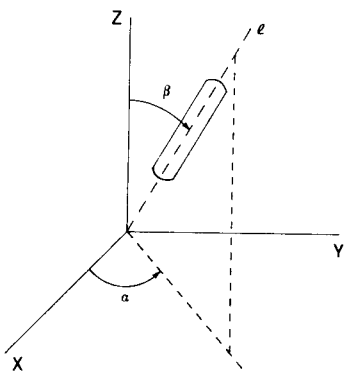

Fig. 2.1. The two angles specifying the orientation of a cylindrically symmetric molecule.

account. We shall come back to this point later on. The complete static information about the system is represented by its configuration, i.e. by the set of positions r_i and orientations Ω_i of all the particles. The orientation of each cylindrical particle can be determined by two polar or Euler [25] angles (α, β). A knowledge of the enormous number of positional and orientational coordinates specifying the various configurations is fortunately unnecessary if we are only interested in calculating average properties. Suppose for example that the distribution giving the probability for a molecule to have a certain position $(\mathbf{r} + d\mathbf{r})$ and orientation $(\Omega + d\Omega)$, $P^{(1)}(\mathbf{r}, \Omega)$, is known. In this case the average of any property $A(\mathbf{r}, \Omega)$ relating to a single molecule can be calculated as [23]

$$\langle A \rangle = \int d\mathbf{r}\, d\Omega\, A(\mathbf{r}, \Omega) P^{(1)}(\mathbf{r}, \Omega)/N \tag{2.1}$$

where the integrals over $d\mathbf{r} = dx\, dy\, dz$ and $d\Omega = d\alpha \sin\beta\, d\beta$ extend respectively to the sample volume V and to the angular measure, here 4π, while the angular brackets denote an ensemble average. The factor of $(1/N)$ in Eqn. 2.1 comes from the normalization of the distribution $P^{(1)}(\mathbf{r}, \Omega)$ to the total number of particles N.

The one-particle or singlet distribution $P^{(1)}$ therefore contains all the microscopic information necessary to calculate one particle properties. In turn the structure and ordering of the system will be reflected by $P^{(1)}$. Ideally a complete statistical description of one particle properties would be obtained by studying the singlet distribution in various phases and examining its changes at the various phase transitions. For a uniform fluid, e.g. a nematic liquid crystal, where there exists long range orientational but not positional order, the singlet probability will be independent on the position of molecules relative to the laboratory frame:

$$P^{(1)}(\mathbf{r}, \Omega) = \rho P(\Omega) \tag{2.2}$$

where $\rho = N/V$ is the number density and $P(\Omega)$ is a purely orientational distribution normalized to unity, i.e.

$$\int d\Omega\, P(\Omega) = 1$$

For an ordinary isotropic fluid $P(\Omega)$ does not depend on the molecular orientation and therefore it must be a constant, $P(\Omega) = 1/(4\pi)$.

Notice, however, that a membrane bilayer is not uniform. Even neglecting the important heterogeneities in the bilayer plane we have changes across the bilayer, i.e. along our z axis. Thus we have a positional-orientational

distribution $P^{(1)}(z, \Omega)$. This is not normally adopted and a purely orientational distribution is implicitly employed. This can be done in two limiting situations. One is when we probe the whole bilayer at once. In this case we really consider

$$P(\Omega) = \int dz\, P(z, \Omega)$$

Experimentally this situation can arise e.g. when using a probe with size comparable to the bilayer thickness. Another, different case is that of a probe that ideally reports the situation of the bilayer at a certain depth z. In this case the ordering information obtained, as described later on, will be a local one. An approximation to this idealized situation is obtained with probes like the anthroyl stearic acids (AS) which, when ionized, anchor with their carboxylic group to the polar heads in the bilayer surface, while having the chromophoric group at a certain depth z_0 inside [24]. Having said this we can limit ourselves to considering the purely orientational distribution $P(\Omega)$ for a mono-bilayer and exploit the formal similarity with that of a uniformly aligned nematic with the director along, say, the z direction. As mentioned already this is a function of the two polar angles giving the molecular orientation of the particle in question i.e.

$$P(\Omega) = P(\alpha, \beta)$$

if our molecules have cylindrical symmetry. The detailed form of $P(\Omega)$ is of course unknown, but some constraints imposed on it by symmetry can nevertheless be easily taken into account. We know from experiment that the symmetry of the mesophase is uniaxial, i.e. that rotating the sample about z nothing changes. This means that the probability for a molecule to have orientation $\Omega = (\alpha, \beta)$ should be the same whatever the angle α. More concisely

$$P(\alpha, \beta) = P(\beta)/2\pi \tag{2.3}$$

Another experimental finding is that turning the aligned sample upside down nothing changes. Thus we should have

$$P(\beta) = P(\pi - \beta) \tag{2.4}$$

This is quite reasonable if we think of the molecules of interest as spherocylinders (cf. Fig. 2.1) or other cylindrically symmetric objects where head and tail are not distinguishable. Our distribution should also be re-normalized, so that

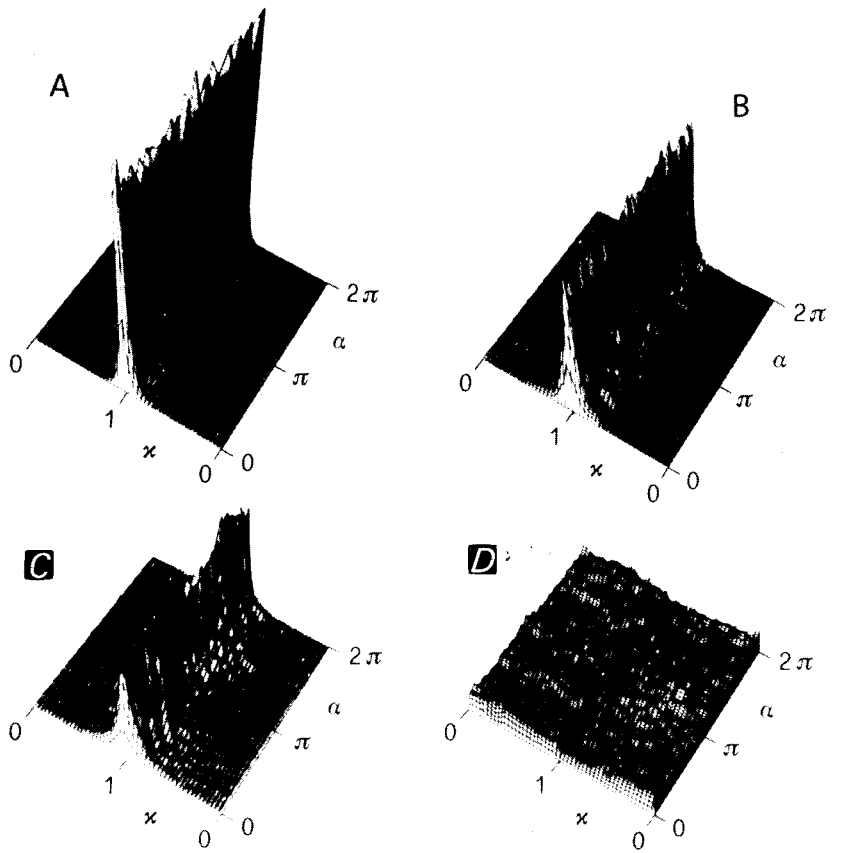

Fig. 2.2. A histogram of the singlet distribution function $P(\alpha, x)$, $x = |\cos\beta|$ for a $10 \times 10 \times 10$ lattice of particles studied with the molecular dynamics methods [26]. Particles on sites i and j interact with the nearest neighbour potential $U_{ij} = -\varepsilon P_2(\cos\beta_{ij})$. Distributions shown for reduced temperatures $kT/\varepsilon = 0.50$(A), 0.79(B), 0.88(C) and 1.30(D).

$$\int d\beta \sin\beta P(\beta) = 1 \tag{2.5}$$

In Fig. 2.2 we show as an example the full singlet orientational distribution obtained using the molecular dynamics method of computer simulation of a simplified model of oriented system [26].

In a real experiment it will be extremely difficult to get complete information on the distribution $P(\Omega)$. A useful approach, however, is that of trying to approximate $P(\Omega)$ in terms of a set of quantities that we can obtain from experiment. We need for this a set of functions orthogonal when integrated over $d\beta \sin\beta$. Such a set of functions is that of Legendre polynomials [27], $P_L(\cos\beta)$, for which we have

TABLE 2.1

THE EXPLICIT FORM OF THE FIRST SIX LEGENDRE POLYNOMIALS $P_L(\cos\beta)$

$P_0(\cos\beta) = 1$	$P_3(\cos\beta) = (5\cos^3\beta - 3\cos\beta)/2$
$P_1(\cos\beta) = \cos\beta$	$P_4(\cos\beta) = (35\cos^4\beta - 30\cos^2\beta + 3)/8$
$P_2(\cos\beta) = (3\cos^2\beta - 1)/2$	$P_5(\cos\beta) = (63\cos^5\beta - 70\cos^3\beta + 15\cos\beta)/8$

$$\int d\beta \sin\beta P_L(\cos\beta)P_N(\cos\beta) = \frac{2}{2L+1}\delta_{LN} \tag{2.6}$$

The explicit form of these Legendre polynomials is really very simple and the first few terms are given in Table 2.1, while in Fig. 2.3 we show a graph of $P_2(\cos\beta)$ and $P_4(\cos\beta)$ versus $\cos\beta$.

Legendre polynomials have the useful property that $P_L(\cos\beta)$ is an even function of $\cos\beta$ if the rank L is even and an odd function if L is odd

$$P_L(\cos\beta) = (-)^L P_L(-\cos\beta) \tag{2.7}$$

Since $\cos(\pi - \beta) = -\cos\beta$ this means that in writing the orientational distribution in terms of $P_L(\cos\beta)$ functions only even L terms need to be retained. Thus we can write

$$P(\beta) = \sum f_L P_L(\cos\beta) \qquad L \text{ even} \tag{2.8}$$

Multiplying both sides of Eqn. 2.8 by $P_N(\cos\beta)$ and integrating over $\sin\beta\, d\beta$:

$$\int P(\beta)P_N(\cos\beta)\sin\beta\, d\beta = \sum f_L \int P_L(\cos\beta)P_N(\cos\beta)\sin\beta\, d\beta \tag{2.9a}$$

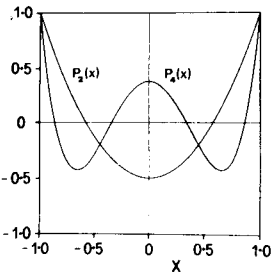

Fig. 2.3. The second and fourth rank Legendre polynomials $P_2(x)$ and $P_4(x)$ plotted as a function of $x = \cos\beta$.

we find the coefficients in Eqn. 2.8 as

$$f_N = \frac{2N+1}{2}\langle P_N\rangle \tag{2.9b}$$

where we have used the notation

$$\langle P_N\rangle = \int d\beta \sin\beta\, P_N(\cos\beta)P(\beta) \tag{2.10}$$

The averages $\langle P_N\rangle$ represent our set of orientational order parameters [23]. The knowledge of the (infinite) set of $\langle P_N\rangle$ would completely define the distribution. We can write

$$P(\beta) = 1/2 + (5/2)\langle P_2\rangle P_2(\cos\beta) + (9/2)\langle P_4\rangle P_4(\cos\beta) + \ldots \tag{2.11}$$

The first term contains the second rank order parameter

$$\langle P_2\rangle = \frac{3}{2}\langle\cos^2\beta\rangle - \frac{1}{2} \tag{2.12}$$

It is easy to see that $\langle P_2\rangle$ has some properties that we would intuitively expect an order parameter to possess. For a system of perfectly aligned molecules where $\beta = 0$ for every molecule $\langle P_2\rangle = 1$. At the other extreme, for a completely disordered system such as an ordinary isotropic fluid we have

$$\langle\cos^2\beta\rangle = \int d\beta \sin\beta\cos^2\beta \Big/ \int d\beta \sin\beta = 1/3 \tag{2.13}$$

and therefore for a disordered system we find $\langle P_2\rangle = 0$. On going from an ordered to a disordered system the order parameter jumps discontinuously to zero if the transition is of the so called first order type, i.e. if it is associated with an entropy jump. At a continuous, second order transition the change in order parameter is instead a smooth function of temperature. Usually there are also pre-transitional variations in the isotropic phase. We shall see later on that the second rank order parameter $\langle P_2\rangle$ is proportional to the fluorescence polarization anisotropy. This anisotropy can therefore be used to monitor orientational phase transitions [28].

Quite similarly to what we have just said, the higher order parameters $\langle P_4\rangle$, $\langle P_6\rangle$, etc. are, respectively, one for complete order and zero for an isotropic system. We may perhaps ask if there is therefore an advantage in considering more than one order parameter [29]. That this is the case becomes apparent if we refer to Fig. 2.3 where the angular variation of the

Legendre polynomials $P_2(\cos\beta)$ and $P_4(\cos\beta)$ is shown as a function of $\cos\beta$. As we can deduce from Fig. 2.3, if we measure $\langle P_2\rangle$ and find that $\langle P_2\rangle > 0$, this will mean that the majority of molecules has a long axis orientation β between zero and the so-called magic angle, $\beta \sim 54.7°$, or $\cos^{-1}(1/\sqrt{3})$ the zero of $P_2(\cos\beta)$. If, on the other hand, $\langle P_2\rangle < 0$, then we may expect that, on average, molecules will have an orientation giving a negative P_2 (e.g. β between 54.7° and 90°). Let us now consider P_4 and $\langle P_4\rangle$. The zeros of P_4 between 0° and 90° fall at $\beta \sim 30.5$ and 70.1. Suppose we have now measured $\langle P_2\rangle$ and $\langle P_4\rangle$ with some experimental technique. If $\langle P_2\rangle > 0$ and $\langle P_4\rangle > 0$ then the distribution of orientations will be such that the majority of molecules has a long axis orientation between 0° and 30.5°. An example of distribution function of this type is reported in Fig. 2.4.

We might, however, find a positive $\langle P_2\rangle$, as before, and a negative $\langle P_4\rangle$. This would suggest a different type of orientational distribution, e.g. possibly a tilted one with a peak between 30.5° and 54.7°. The qualitative physical significance of other combinations of order parameters can be deduced in a similar way. What we have just said could be extended if we knew $\langle P_6\rangle$ etc. Every higher order parameter restricts the bounds on $P(\cos\beta)$ and thus increases our knowledge on the system [30]. This does not mean, of course, that the expansion in Eqns. 2.8, 2.11 is so rapidly convergent that we only need the first few terms to reconstruct $P(\beta)$. Actually this will not be the case, at least in general. On the other hand a knowledge of $\langle P_4\rangle$ as well as of $\langle P_2\rangle$ can be very useful in discriminating between various models of molecular organization inside the bilayer. To examine this important point we assume that every molecule is moving in an effective potential created by all the other molecules in the system $U(\cos\beta)$.

This effective potential, or pseudopotential, or potential of mean torque [31, 32] will obey the same symmetry restrictions introduced before for the singlet distribution. Thus it will be possible to approximate it as

$$U(\cos\beta) = \sum c_L P_L(\cos\beta) \tag{2.14}$$

This effective potential can in turn be used to calculate order parameters etc. using the Boltzmann expression [33]

$$P(\Omega) = \exp\{-U(\Omega)/kT\} \Big/ \int d\Omega \exp\{-U(\Omega)/kT\} \tag{2.15}$$

where k is the Boltzmann constant, T the absolute temperature and Ω gives the molecular orientation. Thus, e.g.

$$\langle P_2\rangle = \int d\beta \sin\beta\, P_2(\cos\beta) \exp\{-U(\cos\beta)/kT\} \Big/ \int d\beta \sin\beta \exp\{-U(\cos\beta)/kT\}$$

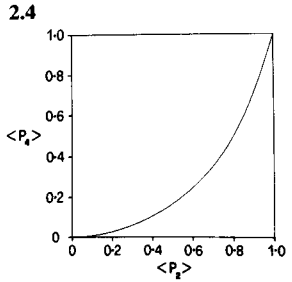

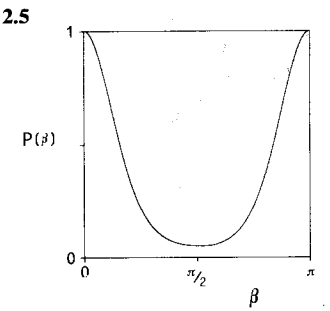

Fig. 2.4. An example of orientational distribution function $P(\beta)$ corresponding to $\langle P_2\rangle > 0$ and $\langle P_4\rangle > 0$ (arbitrary units) plotted as a function of the angle β between molecule and mesophase symmetry axis.

Fig. 2.5. The fourth rank order parameter $\langle P_4\rangle$ versus the second rank order parameter $\langle P_2\rangle$ calculated employing the second rank potential (Eqn. 2.17) in the Boltzmann average (Eqn. 2.15).

The coefficients c_L are proportional to the strength of the solute-solvent interaction between the probe molecule and the surrounding solvent molecules forming the anisotropic phase. They express the aligning potential acting on the probe. It is quite intuitive, and it can also be proved using a mean field theory for mixtures [31], that the coefficients c_L will be proportional to the rank L order parameter for the solvent and to a solute-solvent interaction coefficient, u_L. If the probe concentration is vanishingly small, one has [34]

$$U(x) = kT \sum_L u_L \langle P_L\rangle P_L(x) \qquad L \text{ even} \qquad x = \cos\beta \tag{2.16}$$

Consider as an example one of the most popular models of orientational ordering, i.e. the so-called Maier-Saupe model [35]. This was originally proposed for nematic liquid crystals formed of molecules interacting via attractive and anisotropic London dispersion forces treated according to a molecular field theory. It corresponds, in the general expansion seen above, to a truncation of the series to the first symmetry allowed term, i.e. [31]

$$U(x) = kTu_2\langle P_2\rangle P_2(x) \tag{2.17}$$

This truncation is consistent not just with a dispersion-forces interaction but with any second rank type anisotropic interaction, whatever its physical origin. Indeed the simple interaction, Eqn. 2.17, has proved to be amazingly successful in describing ordering in thermotropic liquid crystals [36]. One interesting point is that calculating order parameters using Eqn. 2.17 we cannot get $\langle P_4\rangle$ to become negative. In Fig. 2.5 we show the order parameter $\langle P_4\rangle$ against $\langle P_2\rangle$ calculated for the Maier-Saupe-like potential. Since the

potential Eqn. 2.17 contains only one parameter, plotting $\langle P_4 \rangle$ versus $\langle P_2 \rangle$ gives a universal curve, without adjustable parameters.

It is therefore quite clear that if we wish to investigate the validity of using the Maier-Saupe-like distribution in describing ordering in a certain anisotropic we should try to calculate not only $\langle P_2 \rangle$ but $\langle P_4 \rangle$ as well. One of the aims of this paper will be to examine in detail when this is possible.

On the same lines measurements of second and fourth rank order parameters may allow testing of theories of structure and conformational mobility in a membrane bilayer [37–39]. In this case it would be best of course to obtain $\langle P_2 \rangle$ and $\langle P_4 \rangle$ along the chain i.e. at various positions inside the bilayer. An example of this type of application is the testing [40] of the *gauche-trans* model put forward by Seelig [41].

2.1.1. Deviation from cylindrical symmetry

We have assumed up to now that our probe molecule has effective cylindrical symmetry, i.e. that only one order parameter $\langle P_L \rangle$ is sufficient to specify ordering at rank L. This is often a good approximation and indeed one that has been up to now universally used in FD studies. It is, however, just an approximation and as data become more precise it may well be no longer satisfactory. This has already happened in NMR studies of molecules dissolved in liquid crystals [42]. There the assumption of cylindrical symmetry was used for a long time, while now full consideration is made of the fact that a molecule may be e.g. lathe-like rather than cylindrically symmetric. Here we shall briefly introduce the additional order parameters necessary to describe such a molecule. We consider the solvent phase to be uniaxial so that an Euler angle α specifying the rotation angle around the director will not be needed. We then write down a general expansion for the probability distribution of finding a molecule in an angular volume element $\beta + d\beta$, $\gamma + d\gamma$ around β, γ.

Here γ is the Euler angle giving the rotation about the molecular long axis necessary to specify the molecular orientation in a laboratory fixed system. The distribution is

$$P(\beta, \gamma) = \sum (2L + 1) f_{Ln} D^{L}_{0n}(0\beta\gamma)/(4\pi) \qquad L \text{ even} \tag{2.18}$$

where the set of Wigner functions $D^{L}_{0n}(0\beta\gamma)$ has been used for the expansion since it provides a complete set over the angular space spanned by β, γ. The coefficients $f_{Ln} = \langle D^{L*}_{0n} \rangle$ represent the new set of order parameters [23]. Notice that the functions $D^{L}_{0n}(0\beta\gamma)$ are essentially spherical harmonics Y_{Ln} (cf. Appendix). Only even terms are allowed as in previous expansion due to the assumed uniaxiality of the mesophase.

To illustrate the significance of the new order parameters let us confine

ourselves to the case of rank $L = 2$ and assume the molecule to be a biaxial object with D_{2h} symmetry, for example anthracene. The existence of a molecular symmetry plane causes only terms with even n to contribute to Eqn. 2.18. The non-vanishing order parameters are therefore

$$\langle D^2_{00}\rangle = \langle P_2\rangle \tag{2.19a}$$

$$\langle D^2_{02}\rangle = \langle D^2_{0,-2}\rangle \tag{2.19b}$$

$\langle D^2_{00}\rangle$ is just the order parameter describing the long axis orientation with respect to the director that we have already seen. $\langle D^2_{02}\rangle$ represents instead a new type of order parameter giving the alignment of the short molecular axis, i.e. of an axis perpendicular to the long axis [32]. In NMR work an alternative notation for order parameters of molecules deviating from cylindrical symmetry is often employed. Instead of second rank order parameters $\langle D^2_{0n}\rangle$ a Cartesian ordering matrix or Saupe matrix S is given,

$$S_{ab} = \langle 3l_a l_b - \delta_{ab}\rangle/2$$

where l_a are the direction cosines of the director in a molecule fixed frame [42]. The two notations are of course equivalent and we report for easy reference in Table 2.2 the relation between the two sets. The Cartesian formulation shows perhaps more intuitively that the secondary order parameter $\langle D^2_{02}\rangle$ refers to the alignment of an axis perpendicular to the long axis.

The variation of the order parameters $\langle D^2_{00}\rangle$ and $\langle D^2_{02}\rangle$ with temperature is quite different as can be shown with a molecular field theory of mesophases formed by non-cylindrically symmetric molecules [32]. In Fig. 2.6 we show this behaviour for various deviations from cylindrical symmetry as obtained from a molecular field calculation where molecules are assumed to interact through a non-axial polarizability tensor $\boldsymbol{\alpha}$. The non-axiality parameter λ is in this case [32] $\lambda = (3/2)^{1/2}(\alpha_{xx} - \alpha_{yy})/[2\alpha_{zz} - \alpha_{xx} - \alpha_{yy}]$. The limiting case of cylindrical symmetry is recovered when $\lambda = 0$. From the point of view of a

TABLE 2.2

THE RELATION BETWEEN THE CARTESIAN ORDERING MATRIX COMPONENT $S_{a,b}$, $a, b = x, y, z$ AND THE WIGNER ROTATION MATRIX AVERAGES $\langle D^2_{mn}\rangle$

$S_{zz} = \langle D^2_{00}\rangle$
$S_{xx} - S_{yy} = (\frac{3}{2})^{1/2}\{\langle D^2_{02}\rangle + \langle D^2_{0-2}\rangle\}$
$S_{xz} = -(\frac{3}{8})^{1/2}\{\langle D^2_{0-1}\rangle + \langle D^2_{01}\rangle\}$
$S_{yz} = i(\frac{3}{8})^{1/2}\{\langle D^2_{01}\rangle + \langle D^2_{0-1}\rangle\}$
$S_{xy} = i(\frac{3}{8})^{1/2}\{\langle D^2_{02}\rangle - \langle D^2_{0-2}\rangle\}$

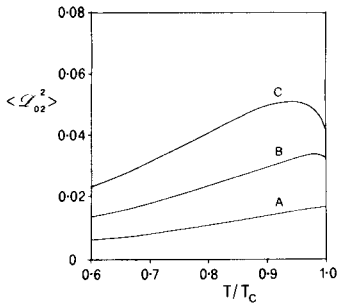

Fig. 2.6. A plot of the secondary order parameter $\langle \mathscr{D}_{02}^2 \rangle = (3/8)^{1/2} \langle \sin^2 \beta \cos 2\gamma \rangle$ versus reduced temperature T/T_c, where T_c is the order-disorder transition temperature, for various values of the deviation from cylindrical symmetry parameter λ.

probing technique, various considerations are important. The first is that when analyzing experimental data a satisfactory theory should tell us when this type of information is going to affect the data and if we can extract it. The other is that the possibility of molecular biaxiality should be taken into account when choosing a particular probe. If we are only interested in long axis ordering then biaxiality could be a nuisance and it may be worth shopping around for a fluorescent probe with vanishingly small deviations. In this respect an estimate of the biaxiality parameter λ from molecular polarizability could be useful. If on the other hand the extra order parameter $\langle D_{02}^2 \rangle$ can be extracted from the experiment, then this information on the short axis alignment may offer additional insight on structure in the bilayer.

The cases treated up to now of cylindrical and biaxial molecules in a uniaxial mesophase are just special cases of a more general description for rigid molecules of any symmetry in a certain ordered phase [23]. In this case $P(\Omega)$ is a function of all the three Euler angles (α, β, γ)

$$P(\Omega) = \sum f_{Lmn} D_{mn}^{L}(\Omega)$$

The expansion coefficients are identified as Wigner rotation matrix averages. We have shown elsewhere how group theoretical methods can be employed in determining the non-vanishing order parameters for molecules of various symmetry [23].

Notice that even if we have accounted for deviations from cylindrical symmetry we still have assumed the molecule studied to be a rigid one. This will not be the case in general, for example if we treat a probe like one of the popular anthroyl stearic acids (AS). In that case all that we say applies to the rigid fluorescent segment we are actually looking at, e.g. the anthracene

chromophore in an AS probe. The ordering of the rigid group of interest will be determined in such a case by the intramolecular as well as by the overall motions. Thus the present treatment can still be applied as long as only the ordering of the rigid part with respect to the laboratory frame is considered sufficient [40]. If instead details of intramolecular flexibility are sought, a more general treatment should be developed [44–46]. Similar arguments apply to the case of intrinsic fluorescent groups attached to proteins or other molecules exhibiting segmental mobility [47–49].

2.2. Orientational dynamics

As shown in the previous section, the description of single particle static orientational properties can be effected in terms of the singlet distribution $P(\Omega)$, and of its expansion coefficients in a suitable basis set, the orientational order parameters. Quite similarly the description of single particle orientational dynamics can be realized in terms of a joint probability distribution function $P(\Omega_0 0; \Omega t)$ [26, 50]. This gives the probability that the orientation of a particle is Ω_0 at time zero and Ω at time t. We consider for the moment a monodomain system with the Z axis along the director.

$P(\Omega_0 0; \Omega t)$ can then be expanded for $t \neq 0$ in a product basis set of Wigner functions, much in the same way as we did for the singlet distribution $P(\Omega)$. We find

$$P(\Omega_0 0; \Omega t) = \sum P^{LL'}_{mnm'n'}(t) D^{L}_{mn}(\Omega_0)^* D^{L'}_{m'n'}(\Omega) \tag{2.20}$$

The expansion coefficients can be obtained by exploiting the orthogonality of the Wigner functions. This gives (cf. Eqn. A7)

$$P^{LL'}_{mn,m'n'}(t) = (2L+1)(2L'+1)\langle D^{L}_{mn}(\Omega_0) D^{L'}_{m'n'}(\Omega)^* \rangle / 64\pi^4 \tag{2.21}$$

Equation 2.20 can be simplified using group theory by requiring the joint probability to be invariant under the various symmetry operations of the mesophase and of the constituent particles. Without going into details of how this is done [23] we only quote here two important results, which are also easy to get by direct inspection. First if the mesophase is uniaxial the requirement of invariance upon rotation about the Z axis yields $\delta_{mm'}$ in Eqn. 2.21. Secondly, if the solute molecule has effective cylindrical symmetry then another selection rule, $\delta_{nn'}$ is obtained [50]. If we confine ourselves to this limiting case the expansion coefficients of the joint distribution are, apart from a factor, the orientational correlation functions

$$G^{LL'}_{mn} = \langle D^{L}_{mn}(\Omega_0) D^{L'}_{mn}(\Omega)^* \rangle \tag{2.22}$$

These orientational correlation functions have a fundamental role in the description of how and how fast a molecule reorients. We shall see later on that FD methods offer in principle a direct route to the determination of some of the most important of these functions, i.e. those of rank two $G^{22}_{mn}(t)$. Even if higher rank and cross rank correlations enter the general dynamic description (Eqn. 2.20) they are not accessible in normal FD studies and we shall concentrate in what follows on the calculation of the second rank functions $G_{mn}(t) \equiv G^{22}_{mn}(t)$, where we also leave the rank labelling superscripts implied.

The calculation of the orientational correlation functions (Eqn. 2.22) has recently been performed for a simplified anisotropic model system using the method of molecular dynamics [26]. However, it should be said from the start that the first principle calculation of these functions is currently out of reach for 'realistic' models. It is therefore necessary to resort to a parametric description. In this approach a set of assumptions on the dynamics are made and the orientational correlation functions are determined in terms of a set of parameters characterizing this motion (e.g. decay times etc.). We start by assuming that the reorientation process is a stochastic Markov process [50–52]. This implies that the joint distribution $P(\Omega_0 0; \Omega t)$ can be written as

$$P(\Omega_0 0; \Omega t) = P(\Omega_0) P(\Omega_0/\Omega t) \tag{2.23}$$

where $P(\Omega_0/\Omega t)$ is the so-called conditional probability or rotational propagator. It gives the probability that, if the molecular orientation is Ω_0 at time zero, it will be Ω at time t. The limiting values of $P(\Omega_0 0/\Omega t)$ for short and long times t can be obtained at once. Thus at time zero we are certain that the orientation Ω is the one we started from and

$$P(\Omega_0/\Omega 0) = \delta(\Omega - \Omega_0)$$

where $\delta(\Omega - \Omega_0)$ is a Dirac delta function. At the other limit the probability of finding the molecule at orientation Ω will be independent on the initial orientation Ω_0 and only depend on the equilibrium probability of Ω itself. Thus

$$\lim_{t \to \infty} P(\Omega_0/\Omega t) = P(\Omega)$$

where $P(\Omega)$ is the equilibrium Boltzmann probability already seen (cf. Eqn. 2.15). By using as definition Eqn. 2.23 the orientation correlation functions can be written as

$$G_{mn}(t) = \int d\Omega_0 P(\Omega_0) D^2_{mn}(\Omega_0) \int d\Omega \, P(\Omega_0/\Omega t) D^2_{mn}(\Omega)^* \tag{2.24}$$

The orientational correlation function calculation is thus reduced to determining $P(\Omega_0/\Omega t)$, as well as $P(\Omega_0)$ and to an integration. Even though the $G_{mn}(t)$ affords a rather complete description of reorientation, very few techniques can yield their full time decay. Therefore it is often expedient to introduce correlation times

$$\tau_{mn} = \int_0^\infty \{G_{mn}(t) - G_{mn}(\infty)\}\, dt/\{G_{mn}(0) - G_{mn}(\infty)\}$$

corresponding to areas under the normalized correlations. The parameters τ_{mn} give an indication of the rapidity of reorientation as we shall see later on.

A useful symmetry relation between the various G_{mn} is [50]

$$G_{mn}(t) = G_{-m-n}(t) = G_{-mn}(t) = G_{m-n}(t) \qquad (2.25)$$

Let us now turn to the calculation of the conditional probability $P(\Omega_0/\Omega t)$. It is known that the conditional probability for a Markov process obeys an integral master equation and that under certain conditions [51] this can be reduced to a differential equation. We shall assume this to be the case and consider in brief two rather different limiting situations.

2.2.1. The strong collision model

The strong collision model [53] represents a process where the molecule of interest undergoes sudden changes in its orientation at time intervals t. The time taken for the transition from one orientation to the other is supposed to be negligible: the orientational probabilities before and after the sudden change (collision) are assumed to be given by the equilibrium Boltzmann distribution. In practice the molecular orientation before and after each collision is assumed to be uncorrelated, as for the case of large angular jumps. Under these conditions the rate of change of the conditional probability $P(\Omega_0/\Omega t)$ is simply

$$\frac{\partial}{\partial t} P(\Omega_0/\Omega t) = \frac{1}{\tau_c}[P(\Omega) - P(\Omega_0/\Omega_t)] \qquad (2.26)$$

where τ_c is a characteristic decay time.

The solution of this first order linear differential equation subject to the initial condition $P(\Omega_0/\Omega 0) = \delta(\Omega_0 - \Omega)$ is

$$\begin{aligned} P(\Omega_0/\Omega t) &= \delta(\Omega - \Omega_0)\exp(-t/\tau_c) + P(\Omega)\{1 - \exp(-t/\tau_c)\} \\ &= P(\Omega) + \{\delta(\Omega - \Omega_0) - P(\Omega)\}\exp(-t/\tau_c) \end{aligned} \qquad (2.27)$$

This conditional probability obviously reduces to the equilibrium probability

for very long times, as it has to. Thus, in general, the correlation function $G_{mn}(t)$ defined by Eqn. 2.24 will reduce to $|\langle D^2_{mn}\rangle|^2$ at very long times. It is easy to calculate the correlation function G_{mn} at any instant of time t employing Eqn. 2.27. This yields for a cylindrically symmetric probe and mesophase

$$G_{mn}(t) = \{\langle D^2_{mn} D^{2*}_{mn}\rangle - \langle P_2\rangle^2 \delta_{0m}\delta_{0n}\} \exp(-t/\tau_c) + \langle P_2\rangle^2 \delta_{0m}\delta_{0n} \tag{2.28}$$

One problem with Eqn. 2.28 is that the use of a single correlation time ignores the anisotropic nature of the solute. If we consider a long rod-like molecule, for example, Eqn. 2.28 assigns the same correlation time to rotations around the long axis and of the long axis itself. Physically we would expect instead reorientation around the long axis to be much easier than the other with, therefore different decay times for correlation functions reflecting these different motions. This deficiency has been empirically removed by assuming [53] that the correlation time depends on n but not m, so that

$$G_{mn}(t) = \{\langle D^2_{mn} D^{2*}_{mn}\rangle - \langle P_2\rangle^2 \delta_{0m}\delta_{0n}\} \exp(-t/\tau_n) + \langle P_2\rangle^2 \delta_{0m}\delta_{0n} \tag{2.29}$$

In practical applications the second subscript of $G_{mn}(t)$ turns out to indicate the component of a certain (2nd rank) tensorial interaction so that this generalized strong collision model allows each component to decay with its own correlation time τ_n. This can be more easily understood by looking at the explicit form of $G_{00}(t)$, $G_{02}(t)$ i.e.

$$G_{00}(t) = \langle P_2[\cos\beta(0)] P_2[\cos\beta(t)]\rangle$$

$$G_{02}(t) = \sqrt{3/8}\langle \sin^2\beta(0) \sin^2\beta(t) \exp[i2\gamma(0)] \exp[-i2\gamma(t)]\rangle$$

where we recall that β is the angle between the director and the molecule symmetry axis while γ refers to a rotation about this symmetry axis. Thus $G_{00}(t)$ only refers to symmetry axis reorientation and the physical significance of the associated decay time τ_0 can be easily understood as that of a long axis reorientation time.

The interpretation of the correlation time τ_2 associated with $G_{02}(t)$ is not so immediate. However, if we are treating a long molecule where the angle β varies much more slowly than γ then the time decay τ_2 of $G_{02}(t)$ will refer essentially to rotations around the molecule axis as shown in Fig. 2.7.

Equation 2.29 can be written in terms of order parameters by coupling the two Wigner rotation matrices as in Eqn. A12. The explicit results are given in Table 2.3.

From what we have said it seems clear that the strong collision model offers a simple empirical form for the orientational correlation function. It

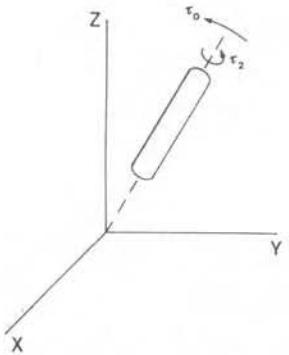

Fig. 2.7. A sketch illustrating the qualitative significance of the orientational correlation times τ_0 and τ_2 (see text).

gives the correct result at zero and infinite time and assumes an exponential decay in between. The strong collision assumption gives the same rate of decay for correlations of various rank. On an intuitive basis we expect this type of reorientation to hold for a solute molecule reorienting in a solvent of bulkier molecules. In this case the collisions with the surrounding molecules might cause the large angular jumps implicit in the model. This finds confirmation at least for isotropic liquids. An opposite limiting situation arises when the solute molecule reorients by small random angular steps, corresponding to the so-called diffusion model.

2.2.2. The diffusion model

In an ordered fluid the reorienting molecule is subjected to random solvent collisions as well as to a systematic ordering torque caused by the

TABLE 2.3

EXPLICIT EXPRESSION FOR THE WIGNER MATRIX CORRELATION FUNCTIONS INITIAL VALUES $G_{mn}(0) = \langle D^2_{mn} D^{2*}_{mn} \rangle$ IN THE CASE OF CYLINDRICALLY SYMMETRIC PROBE AND UNIAXIAL MESOPHASE

m	n	$G_{mn}(0) = \langle D^2_{mn} D^{2*}_{mn} \rangle$
0	0	$1/5 + 2\langle P_2 \rangle/7 + 18\langle P_4 \rangle/35$
±1	0	$1/5 + \langle P_2 \rangle/7 - 12\langle P_4 \rangle/35$
±2	0	$1/5 - 2\langle P_2 \rangle/7 + 3\langle P_4 \rangle/35$
0	±1	$1/5 + \langle P_2 \rangle/7 - 12\langle P_4 \rangle/35$
±1	±1	$1/5 + \langle P_2 \rangle/14 + 8\langle P_4 \rangle/35$
±2	±1	$1/5 - \langle P_2 \rangle/7 - 2\langle P_4 \rangle/35$
0	±2	$1/5 - 2\langle P_2 \rangle/7 + 3\langle P_4 \rangle/35$
±1	±2	$1/5 - \langle P_2 \rangle/7 - 2\langle P_4 \rangle/35$
±2	±2	$1/5 + 2\langle P_2 \rangle/7 + \langle P_4 \rangle/70$

effective aligning potential. Here we introduce and solve the diffusional dynamics equations. If only the final expression for the $G_{mn}(t)$ is of interest (Eqn. 2.41) this part can be omitted.

The equation of motion for the conditional probability for a particle undergoing a rotational Brownian motion subjected to a potential $U(\Omega)$ is, in coordinate free form [50],

$$-\frac{\partial}{\partial t} P(\Omega_0/\Omega t) = \boldsymbol{\Gamma} P(\Omega_0/\Omega t)$$
$$= -\mathbf{J}\left(\mathbf{DJ}\frac{U}{kT}\right)P(\Omega_0/\Omega t) - \mathbf{JDJ}P(\Omega_0/\Omega t) \tag{2.30}$$

This is subjected to the initial boundary condition

$$P(\Omega_0/\Omega 0) = \delta(\Omega - \Omega_0) \tag{2.31}$$

In Eqn. 2.30 $\boldsymbol{\Gamma}$ is called the stochastic operator, $\mathbf{J}$ is formally an angular momentum operator in a particle-fixed frame and in dimensionless form [25] and finally $\mathbf{D}$ is the rotational diffusion tensor of the particle. The single particle potential U is a function of the molecular orientation. When U is a constant, Eqn. 2.30 reduces to the well known equation of rotational diffusion in an isotropic medium [54]; the eigenvalues and eigenfunctions of the stochastic operator are in that case

$$E_{Jn} = D_\perp\{J(J+1) + (D_\parallel/D_\perp - 1)n^2\} \tag{2.32}$$

and

$$\psi_{Jmn}(\Omega) = \left(\frac{2J+1}{8\pi^2}\right)^{1/2} D^{J*}_{mn}(\Omega) \tag{2.33}$$

provided the diffusion tensor is cylindrically symmetric, as we shall assume from now on. The components $D_\parallel$ and $D_\perp$ refer respectively to reorientation around the symmetry axis and around an axis perpendicular to it. Thus we expect $D_\parallel > D_\perp$ for a rod-like molecule (prolate rotator) and $D_\parallel < D_\perp$ for a disk-like one (oblate rotator). The presence of the term containing the potential in Eqn. 2.30 causes in general $\boldsymbol{\Gamma}$ to be non-hermitian. However, it can be shown that, if the detailed balance principle holds, $\boldsymbol{\Gamma}$ can be made Hermitian by the transformation

$$\tilde{\Gamma} = P^{-1/2}\Gamma P^{1/2} \tag{2.34}$$

where P is the equilibrium orientational distribution function and $\tilde{\boldsymbol{\Gamma}}$ is the

Hermitian stochastic operator. The existence of this transformation guarantees that Γ can be diagonalized and that its eigenvalues are real. The eigenvalues of Γ constitute a non-negative sequence; the reciprocal of the eigenvalues are the relaxation or decay times of the process. The first eigenvalue of Γ is always zero, corresponding to the equilibrium probability which, being unaffected by the stochastic operator, has an infinite relaxation time. We shall now examine briefly the unsymmetrized problem, originally solved by Nordio and his group [50, 55]. They express Γ in Euler angles, where it has the form

$$\Gamma P(\Omega_0/\Omega t) = \nabla^2_\Omega P(\Omega_0/\Omega t) + \frac{(\sin\beta)^{-1}}{kT}\,\frac{\partial}{\partial\beta}\sin\beta\, P(\Omega_0/\Omega t)\frac{dU}{d\beta} \tag{2.35}$$

where ∇^2_Ω is the Laplacian in terms of the Euler angles $(\alpha\beta\gamma)$ describing the orientation of the molecule with respect to the director. The operator Γ is then given a representation in a Wigner rotation matrices basis (i.e. as we have seen, the eigenfunctions of $\boldsymbol{JDJ} = \nabla^2_\Omega$). For a cylindrically symmetric probe reorienting in a uniaxial mesophase it is clear that the angular momentum projection pseudo-quantum numbers m and n are still good labels for the eigenvalues of Γ. In other words the total representation of Γ factorizes in diagonal blocks labelled by m and n. In Nordio's notation the (mn) block is called $-D_\perp R^{mn}$ and one has

$$D_\perp^{-1}\frac{d}{dt}C^{mn}_J = \sum_{J'}(R^{mn})_{JJ'}C^{mn}_{J'} \tag{2.36}$$

where the vector C^{mn} is defined through the expansion

$$P(\Omega_0/\Omega t) = \sum C^{mn}_J(t)D^J_{mn}(\Omega) \tag{2.37}$$

The explicit expression for the R^{mn} matrix elements is

$$\begin{aligned}(R^{mn})_{JJ'} &= -[J(J+1) + (D_\parallel/D_\perp - 1)n^2]\delta_{JJ'} \\ &\quad -(1/2)\sum_{L\neq 0} u_L\langle P_L\rangle C(LJ'J;0m)C(LJ'J;0n)\{J(J+1) - J'(J'+1) + L(L+1)\}\end{aligned} \tag{2.38}$$

The parameters u_L are the expansion coefficients for the orientational potential of a molecule (Eqn. 2.16). The axis of symmetry of the diffusion and of the ordering tensors are assumed to coincide. It has been shown [55] that the solution to Eqn. 2.35 subject to the initial condition Eqn. 2.31 is

$$P(\Omega_0/\Omega t) = \sum (2I+1)(\chi^{mn})_{JK}(\chi^{mn})^{-1}_{KI}\exp(D_\perp r^{mn}_K t)D^{I*}_{mn}(\Omega_0)D^J_{mn}(\Omega) \tag{2.39}$$

where χ is the transformation that diagonalizes R:

$$\chi^{-1}\mathbf{R}\chi = \mathbf{r} \tag{2.40}$$

A lower case notation is introduced [4] for the diagonal eigenvalues matrix.

Substituting in Eqn. 2.24, we see that the diffusional correlation functions can be written for a cylindrically symmetric molecule reorienting in a uniaxial mesophase as a series of exponential decays.

$$G_{mn}(t) = \sum (b^{mn})_K \exp(t/\tau^K_{mn}) \tag{2.41}$$

where

$$\tau^K_{mn} = 1/\{D_\perp \rho^{mn}_K t - (D_\parallel - D_\perp)n^2\} \tag{2.42}$$

The pre-exponential coefficients $(b^{mn})_k$ are found to be

$$(b^{mn})_K = (1/5) \sum (2I+1)\langle D^2_{mn} D^{I*}_{mn}\rangle (\chi^{mn})_{2K} (\chi^{mn})^{-1}_{KI} \tag{2.43}$$

where the average $\langle D^2_{mn} D^{I*}_{mn}\rangle$ can be expressed in terms of order parameters using Eqn. A12.

The solute-solvent interaction coefficients u_L give the expansion for the effective potential acting on a probe molecule with its axis at an angle β from the director as we have seen in Eqn. 2.16. In the numerical calculations we restrict ourselves to the second rank ($L = 2$) term in the expansion, thus getting an effective potential of the Maier–Saupe type as in Eqn. 2.17.

For many practical cases the sum over an infinite number of exponentials in the correlation function expression (Eqn. 2.41) can be truncated to just the first term, giving a decay similar to that expected from a strong collision model, i.e.

$$G_{mn}(t) = \{G_{mn}(0) - G_{mn}(\infty)\} \exp(-t/\tau_{mn}) + G_{mn}(\infty) \tag{2.44}$$

where we have dropped the superscript K on τ^K_{mn}. In Figs. 2.8 and 2.9 we show as an example a plot of the decay times and of the pre-exponential coefficients in the expansion of the correlation $G_{00}(t)$ truncated to the third term. This correlation function refers to motion of the molecule symmetry axis, as we have seen in §2.2.1. As Figs. 2.8 and 2.9 show, the expansion can be quite safely truncated to the first term over a wide range of order parameters $\langle P_2\rangle$ and thus of temperatures. On the other hand, this one exponential approximation is not always satisfactory, especially at relatively high order. We have not mentioned viscosity at all in our treatment of

2.8

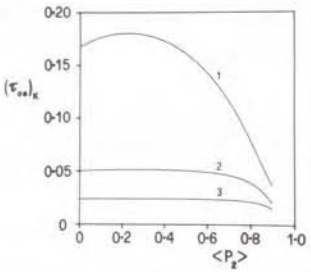

Fig. 2.8. The dependence on the order parameter $\langle P_2 \rangle$ of the first three decay times $(\tau_{00})_K$ in the series expansion for the diffusional correlation function $G_{00}(t)$.

Fig. 2.9. Same as Fig. 2.8 but for the pre-exponential coefficient $(b^{oo})_K$.

rotational dynamics and since this is an often used concept we may wonder where it could come into the picture.

For an ordinary fluid the well known Stokes-Einstein relation links the diffusion tensor to molecular dimensions and to the fluid viscosity η. For a spherical molecule

$$D = kT/(6\pi\eta V) \tag{2.45}$$

with k Boltzmann constant, T temperature and V molecular volume. Slightly more complex expressions hold for anisotropic molecules [54]. If the Stokes-Einstein relation had general validity a determination of D for a molecule of known geometry would allow determination of the molecular volume. However, even for isotropic liquids, application of Eqn. 2.45 often gives inconsistent results. In particular putting in a macroscopic η frequently gives molecular dimensions smaller than the Van der Waals ones [54]. This can be ascribed to the stick boundary conditions implied in deriving Eqn. 2.45. In other words in obtaining the Stokes-Einstein relation it is assumed that the solvent sticks at the solute surface. Different boundary conditions, where the solvent instead 'slips' at the surface have been implemented by Hu and Zwanzig [56] and give a rather conflicting view of rotation, where resistance to angular motion comes from the amount of solvent which the solute has to move around in order to rotate. Without going into details which are inappropriate here it is easy to see that the relation between diffusion coefficient and viscosity is far from obvious even in ordinary fluids.

In an ordered fluid like a liquid crystal or a membrane the situation is further complicated by the fact that the viscosity itself is a tensor, being different in different directions [57]. To the best of our knowledge, a generalization of the Stokes-Einstein relation applicable to anisotropic fluids has not yet been obtained. It seems appropriate therefore to avoid expressing

microdynamics in terms of viscosity and describe instead rotational mobility and more loosely 'fluidity' in terms of diffusion tensor values or correlation times.

Notice that up to now we have not mentioned the problem of deviations from cylindrical symmetry introduced earlier on. This has been treated in a perturbative fashion [58] and can be introduced if necessary. For our purposes here this represents too much of a complication, in view of the fact that dynamic effects of non-cylindrical symmetry are expected to be relatively difficult to observe, separately from static ones. We shall thus retain throughout the assumption that dynamic properties can be satisfactorily described by an effective cylindrical symmetry hypothesis. We have not entered into the problem of what model to use when trying to interpret real experimental data. This will be briefly examined later on.

3. Fluorescent probes

In the previous section we have gone in some detail into the description of the static and dynamic properties of a molecule dissolved in an anisotropic fluid phase. In the next section we shall discuss how to obtain some of the parameters introduced by studying the time dependent and steady state fluorescence polarization. Here, however, we think it is appropriate to define what we mean by fluorescent probes [7b, 8, 24, 59–61] and to examine some of the characteristics they should possess to be useful in the liquid crystal and membrane field.

Fluorescence [62, 63] is a two-step process resulting from absorption of a photon followed by emission from the excited molecule between two states with the same multiplicity. If we assume these processes to be independent we can write the emitted fluorescence intensity from a molecule at time t after excitation as a product

$$I(t) \propto P_{abs}(0)P_{em}(t)F(t) \tag{3.1}$$

where $P_{abs}(t)$, $P_{em}(t)$, $F(t)$ are, respectively, the probability that the molecule is excited, that it emits and that the molecule is still excited at time t [64]. We shall not be much concerned for the moment with the detailed form of the intrinsic fluorescence decay $F(t)$. We can assume, however, that it can be described by an effective characteristic time τ_F. In most practical applications $F(t)$ could be an exponential or a sum of exponentials.

According to perturbation theory [63, 65] the absorption intensity from a weak intensity light source is proportional to the square of the matrix elements $\boldsymbol{\mu} = \langle \psi_0 / \hat{\boldsymbol{\mu}} / \psi' \rangle$ where $\hat{\boldsymbol{\mu}}$ is the dipole moment operator and ψ_0, ψ' are, respectively, the ground and excited state wave function. The transition

moment $\boldsymbol{\mu}$ can be considered a molecular property and for our purposes we can think of it as a unit vector fixed in the molecular frame. Quite similarly the emission intensity will involve an emission transition moment $\bar{\boldsymbol{\mu}} = \langle \psi''/\hat{\boldsymbol{\mu}}/\psi_0 \rangle$, where ψ'' is the wave function of the emitting state. The state ψ'' may be different, in general, from ψ' due e.g. to intramolecular relaxation processes. This means that the transition vectors $\boldsymbol{\mu}$, $\bar{\boldsymbol{\mu}}$ may well not be parallel, but be at a certain angle δ to one another instead. Since we may vary the exciting light wavelength we can to a certain degree choose $\boldsymbol{\mu}$ and therefore vary δ. It has been known for a very long time that the angle δ can be determined by measuring the polarization anisotropy ratio r_0 for the probe of interest dissolved in a transparent frozen medium (a glass) [66]

$$r_0 = (2/5)P_2(\cos \delta) \tag{3.2}$$

In the literature, results are often given in terms of polarization P

$$\begin{aligned} P &= (I_\parallel - I_\perp)/(I_\parallel + I_\perp) \\ &= 3r_0/(2 + r_0) \end{aligned} \tag{3.3}$$

Incidentally, Eqn. 3.2 will come out as a limiting case from the general treatment in the next section.

As the name suggests, a probe molecule has to report information on the environment surrounding it. There are essentially two situations we can consider. One is when we are interested in obtaining information on the substrate. In this case it should be remembered that the information obtained is always second hand, mediated through the solute-solvent interaction coefficients, as discussed earlier. Thus proper care should be taken in ensuring a minimum of perturbation by the probe to the bilayer, and generally in choosing a probe that mimicks as far as possible one of the constituents of the membrane system. Another possibility, however, is that we are interested in the behaviour of a foreign solute molecule in the system. Thus the behaviour of, say, cholesterol in the membrane can be investigated by choosing a probe that resembles this solute as far as possible. If this second type of situation is of interest, the perturbation to the system by the probe is something that is inherent to the problem studied rather than an undesired side effect.

From the point of view of simplifying, or even making possible at all an analysis of the results obtained from a polarization anisotropy investigation, there are some optimum characteristics that a fluorescent probe ought to possess. These 'desiderata' mainly follow from the need to properly describe the molecule we are using as a reporter.

A first, rather obvious and yet often neglected requirement is that the

molecule used should be well characterized from the spectroscopic point of view. Its transition moments, quantum yield, the polarization of the bands of interest, the existence or not of pronounced solvent and temperature effects should be known [62]. It is important to have an idea of the fluorescence lifetimes in a system with characteristics similar to the one that is under investigation. The relative time scales of the fluorescence decay and the reorientation should be such as to render order parameter and possibly dynamic parameters observable [4, 19]. It is convenient to choose a probe that is rigid and that has a shape deviating significantly from a spherical one, such as a rod-like or a disk-like shape. A cylindrical symmetry or at least a well-defined symmetry (e.g. biaxial) is an advantage. In this way information on the ordering can be more easily obtained. The probe should of course have characteristics of chemical, thermal and photochemical stability under the conditions of the experiment. It is important to know the properties of the probe that determine its partitioning in the system [24] (e.g. if the probe is charged, hydrophilic, lipophilic). The specific interactions of the probe can be turned to advantage here since they may allow selective investigation of portions of the membrane.

From this long list it seems clear that it is next to impossible to find an ideal probe possessing all the desired properties. In practice a relatively small number of probes are used in the great majority of polarization studies. We shall consider here in some detail two of the probes most commonly used in membrane investigations. We shall see that even for these supposedly well-known probe molecules further spectroscopic investigations are needed.

3.1.1,6-Diphenylhexatriene (DPH)

DPH [24, 61, 67–74] is certainly one of the most popular probes for studying membrane fluidity [10–13, 16, 24, 59] (cf. §5). It is a fairly rigid, elongated molecule, about 13 Å long, planar in the ground state (Fig. 3.1). It

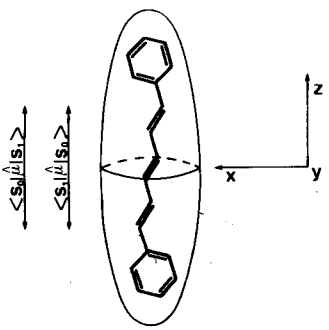

Fig. 3.1. The molecular structure of DPH together with the molecular axis system employed.

is normally assumed to have cylindrical symmetry. While this seems to be a reasonable assumption, it is also one that is waiting confirmation, e.g. from NMR studies of the second rank order parameters.

In view of its universal use DPH might be expected to have predictable and well characterized spectroscopic properties. This is not quite the case and indeed the photophysics of DPH presents several remarkable and unusual features, e.g. when compared to condensed aromatic ring systems, whose interpretation is still the subject of active controversy [70–74]. Here we wish to give a brief discussion of those aspects of DPH spectral properties that should be kept in mind when using it as a probe. To establish notation we recall that an undistorted DPH molecule belongs to the C_{2h} point group, which has four possible representations, A_g, A_u, B_g and B_u [65]. The ground singlet state S_0 belongs to the totally symmetric ^1A_g representation, and the (π, π^*) states are either $^1B_u^*$ or $^1A_g^*$. The first two excited singlets, S_1 and S_2 are invariably (π, π^*) states in aromatic hydrocarbons [62], so that in DPH their symmetry is either $^1B_u^*$ or $^1A_g^*$. The $^1B_u^* \leftrightarrow {}^1A_g$ transition is symmetry allowed, while the $^1A_g^* \leftrightarrow {}^1A_g$ transition is forbidden. On the experimental side we recall that DPH absorbs light in near UV and it emits with very high quantum yield in the blue region of the visible spectrum. In Fig. 3.2 we show the absorption spectrum of DPH in three organic solvents of different polarity.

The absorption spectrum changes as the polarity and refractive index of the solvent change. This fact and the high absorption coefficient of the absorption maximum ($\varepsilon_{430} \sim 80\,000\,\mathrm{l\,cm^{-1}\,mol^{-1}}$) have been associated with the strong transition moment of the fully allowed $\pi \rightarrow \pi^*$ band. Differing from the absorption spectrum, the emission spectrum of DPH changes very little with a change in solvent. In particular the emission maximum is relatively insensitive to changes in polarity, viscosity and temperature [73]. The

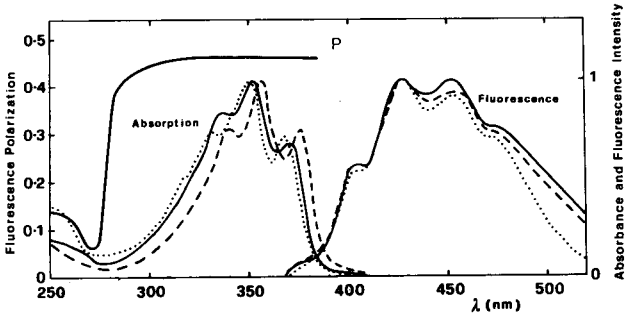

Fig. 3.2. The absorption and fluorescence spectrum of DPH in various organic solvents: ethanol(—); dioxane (---); hexane (· · ·). Also shown is the polarization of fluorescence $P = (I_\parallel - I_\perp)/(I_\parallel + I_\perp)$ as a function of wavelength determined in polypropylene glycol at $T = -50°C$ [79].

emission spectra has therefore been assigned to a weak transition [71]. Another characteristic is that the absorption and emission spectra fail to show a good 'mirror symmetry'; the emission spectrum is rather structureless and shows little overlap with the absorption spectrum. In general this behaviour follows from differences between the nuclear configurations in the ground state and in the first singlet excited state [75]. The radiative lifetimes obtained through the relation $\tau_{RAD} = \tau_F/q$ where τ_F is the experimental fluorescence decay time and q the quantum yield, differ markedly from the ones obtained from the Strickler-Berg equation [76] which relates fluorescence lifetimes to absorption intensities. This behaviour is normally shown by compounds that present distortions in the mirror symmetry relationship [75]. The experimental radiative lifetimes in aromatic and aliphatic solvents differ widely. For instance τ_{RAD} in cyclohexane is 15.5 ns, while it is only 8.6 ns in benzene. The solvent refractive index dependence alone seems unable to explain the effect. The radiative lifetimes increase with temperature in various solvents while being essentially constant in propyleneglycol [70].

For probe applications it is interesting to notice that the fluorescence lifetime τ_F changes quite sensibly when changing solvent, especially when the solvent polarity varies [68]. In Table 3.1 we report the results obtained by various authors for the decay time of DPH in a number of solvents.

The complex behaviour of DPH can be attributed in general to the fact that its two excited singlet states are very near in energy (800 cm^{-1} for DPH in hexane [72]) so that their relative position can be affected by perturbations induced by solvent polarity for example, or even by conformational changes in the excited state. There have been, however, a number of models and conflicting interpretations put forward in the literature about the assignment and the characteristic of the emitting state [72–74]. The argument has now been going on for some 20 years. A turning point was provided by the theoretical calculations of Schulten and Karplus [80] who showed that the lowest excited state in polyenes with $N > 2$ is of the $^1A_g^*$ type. Mixing of the excited states linked to a conformational change has been invoked [71]. It is clear that in this case the dipole may vary with an effect on the polarization as we shall see in the next section.

The fluorescence decay of DPH in organic solvents has been reported to be always mono-exponential [67]. A bi-exponential decay for DPH in ethanol at −25°C has however been found by Birch and Imhof [81].

We now move to the other characteristic of DPH as a fluorescent probe. A useful property is that DPH has well separated absorption and emission bands, which limits the probability of secondary absorption of the emitted photons and makes possible an effective filtering off of the residual excitation light.

The fluorescence decay of DPH has been found to be temperature

TABLE 3.1

FLUORESCENCE DECAY TIMES τ_F FOR DPH IN SOLVENTS OF DIFFERENT DIELECTRIC CONSTANT ε AND VISCOSITY η [77,78]

Where available reorientational diffusion times τ_R and initial values of the polarization anisotropy decay r_0 (cf. §4) have also been reported.

Solvent	ε	T(°C)	τ_F(ns)	η(cP)	r_0	$\tau_R = \frac{1}{6D_\perp}$(ns)	Refs.
n-Hexane	1.89	25	15.7 ± 0.2	0.29			[68]
3-Methyl pentane	1.91	20	15.4	0.37			[68]
n-Heptane	1.92	22	15.6 ± 0.2	0.39			[68]
Cyclohexane	2.02	20	12.4	1.00			[61]
Methyl cyclohexane	2.02	20	13.5 ± 0.2	0.73			[68]
Perfluoro-*n*-hexane		25	32.5 ± 0.5	0.67			[68]
1,4-Dioxane	2.21	25	7.8 ± 0.1	1.20			[68]
Benzene	2.28	20	6.1 ± 0.1	0.65			[68]
Chloroform	4.81	20	6.5	0.58			[107]
Ethanol	24.30	25	5.6	1.07			[71]
Methanol	32.63	25	5.8	0.55			[107]
Liquid paraffin		9.2	9.8	400	0.365	18.0	[9b]
		19.8	9.7	200	0.359	7.5	[9b]
		30.0	9.8	100	0.346	4.3	[9b]
		39.5	9.9	60	0.355	2.4	[9b]
Glycerin		−5	5.6	~16000	0.395	448.1	[9b]
	41.14	20	3.9	1200	0.392	95.5	[9b]

independent for large temperature intervals in low dielectric constant solvents [67]. On the other hand there is a temperature variation in polar solvents [67]. It seems that these variations have often been neglected in steady state and time dependent FD measurements in membranes.

3.2. Perylene

Perylene is a flat aromatic molecule with a shape roughly approximating that of a disk with a diameter of 8 Å (Fig. 3.3). It is convenient to choose the molecular z axis for perylene perpendicular to the ring so as to accentuate its near cylindrical symmetry about the short D_{2h} axis.

Since perylene will presumably align with the ring parallel to the director when dissolved in an ordered phase, we expect its order parameter $\langle P_2 \rangle$ to be negative (cf. §2.1). The absorption spectrum of perylene (Fig. 3.4) presents two main, well structured, transitions [61] corresponding to two transition moments lying in the ring plane and perpendicular to one another (Fig. 3.3a). The fluorescence spectrum of perylene in ethanol is reported in Fig. 3.4. The emitting state has the transition moment parallel to the molecular x axis [82]. The polarization spectrum of perylene in propylene glycol [16b, 83] at −50°C also shown in Fig. 3.4 indicates that the angle between absorption

Fig. 3.3. (a) The molecular structure of perylene together with the direction of the transition moments competing for the first two transitions and the assumed molecular axis system. (b) The disk-like shape assumed for perylene.

and emission moments varies with the excitation wavelength. The polarization value of $P \sim 0.5$ at $\lambda = 410$ nm indicates parallel oscillators. On the other hand excitation at $\lambda = 252$ nm corresponds to $P = -0.27$ thus indicating transition moments essentially perpendicular to each other. Intermediate values can be obtained, e.g. at $\lambda_{ex} = 314$ nm a value of $P \sim 0.14$ is found, corresponding to an angle between absorption and emission dipoles of 45° [16b]. This interesting feature allows different types of molecular rotation to be studied in turn. It has been used in anisotropic rotation investigations of organic solvents [82, 84] and model membranes [16b, 85] and internal motion in DNA [86].

The absorption spectrum and the molar extinction coefficient of perylene are relatively insensitive to variations in the solvent dielectric constant. Similar behaviour is shown by the emission spectrum even though small solvent dependent variations have been reported [87]. In view of this perylene is not suitable as a polarity probe for the membrane bilayer. Because of its lipophilicity perylene is assumed to penetrate the non-polar region of the bilayer.

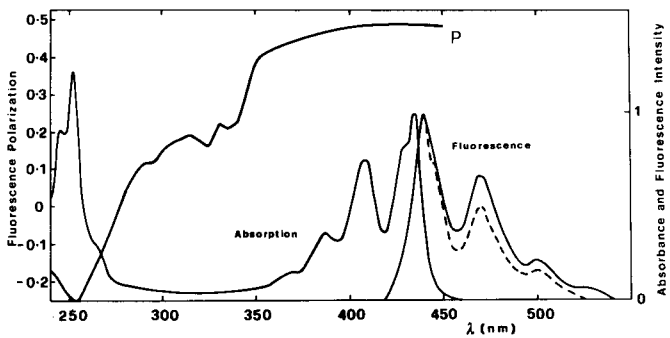

Fig. 3.4. The absorption and emission spectrum of perylene in ethanol (—), dioxane (---), hexane (· · ·). The spectra in ethanol and dioxane are superimposable. Also shown is the polarization P as a function of wavelength for perylene in frozen propylene glycol at $T = -50$°C [83].

The absorption and emission spectrum of perylene overlap sensibly and exhibit a good mirror symmetry. This suggests that the nuclear configuration is basically the same both in the ground and excited state. It also indicates the absence of relatively complex photochemical pathways like those for DPH.

Non-single exponential behaviour has been found in dipalmitoyllecithin and egg lecithin dispersions [16b]. Typical average decay times in organic solvents [61, 75, 82, 88–90] vary from 4.7 ns in paraffin [82] to 7.5 ns in benzene [61].

4. Fluorescence depolarization theory

Our aim here is to derive general model-independent expressions for the fluorescence polarization decay. By separating the geometric and the molecular part of the problem we shall show that a unique formalism can be applied to a variety of experiments on uniformly aligned systems [4] and their angular dependence [91, 92] as well as to experiments on spherical vesicles [19] and biological membranes [93]. We shall then show the theoretical decay curves predicted on the basis of the reorientation models introduced earlier on for a DPH-like and a perylene-like probe. To start with we need to recall the origins of the fluorescence polarization phenomenon.

In an idealized fluorescence depolarization experiment an instantaneous pulse of light, plane polarized in a certain direction $\boldsymbol{e}_i$, impinges on the sample containing the probe molecules. The emitted light is then collected in another direction through an analyzer, set at a direction of polarization $\boldsymbol{e}_f$. In such an idealized experiment the fluorescence intensity at time t, i.e. after a time t has elapsed from the initial pulse, is given by [64]

$$I_{if}(t) = \langle |\mathbf{e}_i \cdot \boldsymbol{\mu}(0)|^2 |\mathbf{e}_f \cdot \bar{\boldsymbol{\mu}}(t)|^2 \rangle F(t) \tag{4.1}$$

where an isotropic fluorescence decay $F(t)$ has been assumed. Here $\boldsymbol{\mu}$ and $\bar{\boldsymbol{\mu}}$ are the absorption and emission transition dipole moments. As mentioned in the previous section we can consider here $\boldsymbol{\mu}$, $\bar{\boldsymbol{\mu}}$ as two molecule-fixed unit vectors; we imagine, in general, $\bar{\boldsymbol{\mu}}$ to be different from $\boldsymbol{\mu}$. We can in fact have, for instance, non-radiative electronic relaxation from the initially excited state which can vary if the exciting wavelength varies, to the emitting state which is normally the first excited singlet state. If this is the case, the internal relaxation process leading from the $\boldsymbol{\mu}$ to the $\bar{\boldsymbol{\mu}}$ direction would give rise to a partial depolarization of the emitted radiation. We assume this internal process, if present, to take place on a time scale much faster than our observation time scale. Thus it provides only a time-independent factor affecting the initial value of the intensity and of the polarization anisotropy.

Returning to Eqn. 4.1 we indicate with the angular brackets an ensemble average over all the motions experienced by the probe molecule up to time t. We consider here only rigid molecules and assume that reorientation is the only depolarizing mechanism. We also assume implicitly that reorientation is unaffected by the internal relaxation of the molecule leading from $\boldsymbol{\mu}$ to $\bar{\boldsymbol{\mu}}$. This should be a reasonable approximation in view of the previous assumption that internal processes are settled by the time reorientation is just beginning to be effective. Within this set of assumptions we can rewrite Eqn. 4.1 as

$$I_{if}(t) = \langle |\mathbf{e}_i \cdot \boldsymbol{\mu}(\Omega_0, 0)|^2 |\mathbf{e}_f \cdot \bar{\boldsymbol{\mu}}(\Omega, t)|^2 \rangle F(t) \tag{4.2}$$

when the molecule is excited at an orientation Ω_0 and is observed after a time t at an orientation Ω in the laboratory frame. To simplify the treatment we now make explicit reference to the laboratory coordinate system shown in Fig. 4.1. We assume the director of the liquid crystal, or equivalently our bilayer normal, to be at an angle $\bar{\Omega} \equiv (d - L)$ with respect to the laboratory Z axis. We assume for the moment the exciting light beam to be travelling along the X axis towards the sample, imagined at the centre of the coordinate system. Two common geometries for observation are (a) along the Y axis (perpendicular geometry) and (b) along the X axis (parallel geometry). In any case the polarizers on the incident and emitted light pathway can be placed vertical (V) or horizontal (H). It is convenient to rewrite Eqn. 4.2 in a way that completely separates the geometric and molecular parts of the problem. As we shall see this can be effectively done by first introducing polarization tensors

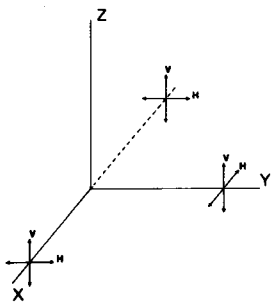

Fig. 4.1. Laboratory coordinate system for a FD experiment. Light polarized parallel (V) or perpendicular (H) to the Z axis impinges on the sample placed at the origin. The emitted fluorescence is observed through a polarizer (a) along the Y axis (perpendicular geometry) or (b) along the X axis (parallel geometry).

$$\mathbf{E}_i = \mathbf{e}_i \otimes \mathbf{e}_i \qquad \mathbf{E}_f = \mathbf{e}_f \otimes \mathbf{e}_f \tag{4.3}$$

which contain the geometrical information about the experiment, and absorption and emission tensors $\mathbf{A}$ and $\bar{\mathbf{A}}$

$$\mathbf{A} = \boldsymbol{\mu} \otimes \boldsymbol{\mu} \qquad \bar{\mathbf{A}} = \bar{\boldsymbol{\mu}} \otimes \bar{\boldsymbol{\mu}} \tag{4.4}$$

containing the spectroscopic information. The notation $\otimes$ indicates a direct product. More explicitly $A_{ij} = e_i e_j$ etc. By expressing Eqn. 4.3 in terms of the irreducible tensor components of the polarization and emission tensors (cf. Appendix), we find the intensity as a sum of contributions labelled by the ranks L, L' of the irreducible components:

$$I_{if}(t) = F(t) \sum_{L,L'} I_{if}^{LL'}(t) \qquad L, L' = 0.2 \tag{4.5}$$

where

$$I_{if}^{LL'}(t) = \sum E_i^{L,m^*} E_f^{L'm'} \langle A_{LAB}^{L,m}(0)\, \bar{A}_{LAB}^{L',m'}(t)^* \rangle \tag{4.6}$$

and $\langle A_{LAB}^{L,m}(0)\, \bar{A}_{LAB}^{L',m'}(t)^* \rangle$ are absorption-emission cross correlation functions. Components of rank one are missing in Eqn. 4.5 since the tensors involved are symmetric. The explicit expressions for the irreducible tensor components can be obtained from Table A1. For convenience we report in Table 4.1 the components of $\mathbf{A}$. Knowing the Cartesian components μ_x, μ_y, μ_z

$$\mu_x = \mu \sin \bar{\vartheta} \cos \bar{\varphi} \tag{4.7a}$$

$$\mu_y = \mu \sin \bar{\vartheta} \sin \bar{\varphi} \tag{4.7b}$$

$$\mu_z = \mu \cos \bar{\vartheta} \tag{4.7c}$$

of a transition moment with polar angles $\bar{\vartheta}$ and $\bar{\varphi}$ in the chosen molecule

TABLE 4.1

IRREDUCIBLE SPHERICAL COMPONENTS OF THE DIRECT PRODUCT TENSOR $\boldsymbol{A} = \boldsymbol{\mu} \otimes \boldsymbol{\mu}$ IN TERMS OF THE CARTESIAN COMPONENTS OF THE VECTOR $\boldsymbol{\mu}$

$A^{0,0} = -(\mu_X^2 + \mu_Y^2 + \mu_Z^2)/3^{1/2}$
$A^{2,0} = (2/3)^{1/2}\{\mu_Z^2 - (\mu_X^2 + \mu_Y^2)/2\}$
$A^{2,\pm 1} = \mp(\mu_X \mu_Z \pm i\mu_Y \mu_Z)$
$A^{2,\pm 2} = (\mu_X^2 - \mu_Y^2 \pm i2\mu_X \mu_Y)/2$

fixed frame, we can work out immediately the irreducible component $A^{2,m}$ using Table 4.1.

To complete the separation between geometric and molecular variables we now transform the transition tensors from the laboratory to a molecular frame. We do this in two steps. We transform first from the laboratory frame shown in Fig. 4.1 to one with z axis parallel to the director (director frame).

$$A^{L,m}_{LAB} = \sum D^{L}_{mq}(d-L)^* A^{Lq}_{DIR} \tag{4.8}$$

and then from the director to the molecule frame. We find

$$A^{Lq}_{DIR} = \sum D^{L}_{qn}(t-d)^* A^{Ln}_{MOL} \tag{4.9}$$

where the notation $D^{L}_{mq}(F'-F)^*$ is employed to indicate the rotation matrix carrying the frame F into F'. Substitution in Eqn. 4.6 gives the intensity components as

$$I^{LL'}_{if}(t) = \sum E^{L,m^*}_{i} E^{L'm'}_{f} A^{Ln}_{MOL}\, \bar{A}^{L'n'^*}_{MOL}$$
$$\times D^{L}_{mq}(d-L)^* D^{L'}_{m'q'}(d-L)\langle D^{L}_{qn}(0-d)^* D^{L'}_{q'n'}(t-d)\rangle \tag{4.10}$$

where we have assumed the director to be fixed in the laboratory frame at least on the experiment time scale. If we now consider the mesophase to be uniaxial in the director frame, symmetry demands $\delta_{qq'}$ in Eqn. 4.10. If we also assume the probe to have effective cylindrical symmetry, the requisite of invariance for a rotation about the molecule axis yields the further restriction $\delta_{nn'}$. We find therefore $I_{if}(t)$ as a sum of four contributions, i.e.

$$I_{if}(t) = \{I^{0,0}_{i,f} + I^{0,2}_{i,f}(d-L) + I^{2,0}_{i,f}(d-L) + I^{2,2}_{i,f}(t, d-L)\}F(t) \tag{4.11}$$

where

$$I^{0,0}_{i,f} = 1/9 \tag{4.12}$$

$$I^{0,2}_{i,f}(d-L) = (1/3)\sum E^{2,m}_{f} D^{2}_{m0}(d-LM)^*\langle P_2\rangle \bar{A}^{2,0^*}_{MOL} \tag{4.13}$$

$$I^{2,0}_{i,f}(d-L) = (1/3)\sum E^{2,m^*}_{i} D^{2}_{mq}(d-L)^*\langle P_2\rangle A^{2,0}_{MOL} \tag{4.14}$$

$$I^{2,2}_{i,f}(t, d-L) = \sum E^{2,m^*}_{i} E^{2,m'}_{f} D^{2}_{mq}(d-L)^* D^{2}_{m'q}(d-L)^* G_q(t) \tag{4.15}$$

We see that only the $I_{if}^{22}(t, d-L)$ contribution is time dependent and carries dynamic information. The molecular information is all contained in the quantity $G_q(t)$,

$$G_q(t) = \sum_n A_{MOL}^{2,n} \bar{A}_{MOL}^{2,n^*} G_{qn}(t) \tag{4.16}$$

while $G_{qn}(t)$ is the usual definition of a Wigner rotation matrix orientational correlation function (cf. Eqn. 2.24)

$$G_{qn}(t) = \langle D_{qn}^2(0-d) D_{qn}^2(t-d)^* \rangle \tag{4.17}$$

Here the generalized spherical harmonic $D_{qn}^L(t-d)^*$ gives the rotation carrying from the director to the molecular frame at time t. We are now in a position to specialize the general model-independent Eqns. 4.12–4.15 to various types of experimental situation.

In practice we shall consider the four intensities obtained by placing the polarizers vertically or horizontally.

(a) Polarizer and analyzer parallel to Z: the required irreducible components of the polarization tensors are

$$E_i^{2,m^*} = (2/3)^{1/2} \delta_{m0} \tag{4.18}$$

$$= E_f^{2,m} \tag{4.19}$$

(b) Polarizer parallel to Z and analyzer parallel to X: the required irreducible component of E_f is:

$$E_f^{2,m} = -(1/6)^{1/2} \delta_{m0} - (\delta_{m2} + \delta_{m-2})/2 \tag{4.20}$$

while the E_i component is given by Eqn. 4.18.

(c) Polarizer parallel to X and analyzer parallel to Z

$$E_i^{2,m} = -(1/6)^{1/2} \delta_{mo} - (\delta_{m2} + \delta_{m-2})/2 \tag{4.21}$$

with E_f coming from Eqn. 4.19.

(d) Polarizer and analyzer parallel to X: these are just Eqns. 4.21 and 4.20.

4.1.1. Monodomain sample [4]

We consider a macroscopically aligned sample with the director parallel to the laboratory Z axis. The rotation carrying the laboratory into the director

frame is in this case a null one, corresponding to the identity. Thus

$$D^2_{mq}(000) = \delta_{mq} \tag{4.22}$$

and we find

$$I^{0,2}_{i,f} = (1/3)E^{2,0}_f \langle P_2 \rangle \bar{A}^{2,0*}_{MOL} \tag{4.23}$$

$$I^{2,0}_{i,f} = (1/3)E^{2,0}_i \langle P_2 \rangle A^{2,0*}_{MOL} \tag{4.24}$$

$$I^{2,2}_{i,f} = \sum_m E^{2,m*}_i E^{2,m}_f G_m(t) \tag{4.25}$$

Substitution of Eqns. 4.12 and 4.23–4.25 in Eqn. 4.11 gives immediately

$$I_{ZZ}(t)/F(t) = 1/9 + (2/3)^{1/2}\langle P_2 \rangle (\bar{A}^{2,0} + A^{2,0})/3 + (2/3)G_0(t) \tag{4.26}$$

$$I_{ZX}(t)/F(t) = 1/9 + \frac{1}{3(6)^{1/2}}\langle P_2 \rangle (2\bar{A}^{2,0} - A^{2,0}) - (1/3)G_0(t) \tag{4.27}$$

$$I_{YZ}(t)/F(t) = 1/9 + \frac{1}{3(6)^{1/2}}\langle P_2 \rangle (2A^{2,0} - \bar{A}^{2,0}) - (1/3)G_0(t) \tag{4.28}$$

$$I_{YX}(t)/F(t) = 1/9 - \frac{1}{3(6)^{1/2}}\langle P_2 \rangle (\bar{A}^{2,0} + A^{2,0}) + (1/6)G_0(t) - (1/2)G_2(t) \tag{4.29}$$

$$I_{XX}/F(t) = 1/9 - \frac{1}{3(6)^{1/2}}\langle P_2 \rangle (A^{2,0} + \bar{A}^{2,0}) + (1/6)G_0(t) + (1/2)G_2(t) \tag{4.30}$$

where we have used the relation

$$A^{2,n*} = (-)^n A^{2,-n} \tag{4.31}$$

which in turn can be easily verified from inspection of Table 4.1.

Our equations show that the equality of Eqns. 4.27 and 4.28 thus of I_{ZX} with I_{YZ} is only obtained if $A^{2,n} = \bar{A}^{2,n}$ i.e. when the absorption and emission transition moments have the same orientation in the molecular frame. The intensities obtained in Eqns. 4.26–4.30 can be combined in various ways for a more convenient comparison with experiment. We consider here explicitly a polarization ratio

$$r(t) = (I_{ZZ}(t) - I_{ZX}(t))/(I_{ZZ}(t) + 2I_{ZX}(t)) \tag{4.32}$$

that can be determined from both a right angle and a parallel geometry experiment. From Eqns. 4.26 and 4.27 we find

$$r(t) = \left\{\frac{1}{6^{1/2}}\bar{A}^{2,0}\langle P_2\rangle + G_0(t)\right\} \Big/ \{1/3 + (2/3)^{1/2}A^{2,0}\langle P_2\rangle\} \tag{4.33}$$

for a cylindrically symmetric probe in a uniaxial mesophase. Within the assumptions of statistical independence of the fluorescence and reorientation processes $r(t)$ depends only on ordering and reorientational dynamics. The polarization ratio in Eqn. 4.33 reduces, in the limit of vanishing order, to the usual one for isotropic liquids [4–10] i.e.

$$r(t) = (I_{\parallel}(t) - I_{\perp}(t))/(I_{\parallel}(t) + 2I_{\perp}(t)) \tag{4.34}$$

where the subscripts refer to the analyzer being set parallel or perpendicular to the exciting light polarization direction.

Limiting expressions for the fluorescence intensities and the polarization ratio $r(t)$ for short times can be derived at once using the results for the initial values given in Table 2.3 for

$$G_{mn}(0) = \langle D^2_{mn}D^{2*}_{mn}\rangle \tag{4.35}$$

As an illustration of the use of Eqns. 4.26–4.30 let us consider the very simple case of a cylindrically symmetric probe with both the absorption and emission transition moments parallel to the symmetry axis. As we discussed in the previous section the fluorescent probe diphenylhexatriene closely approximates such a system. For this type of probe $A^{2,m} = (2/3)^{1/2}\delta_{m0}$ and

$$I_{ZZ}(t)/F(t) = 1/9 + (4/9)\langle P_2\rangle + (4/9)G_{00}(t) \tag{4.36}$$

$$\begin{aligned} I_{ZX}(t)/F(t) &= 1/9 + (1/9)\langle P_2\rangle - (2/9)G_{00}(t) \\ &= I_{YZ}(t)/F(t) \end{aligned} \tag{4.37}$$

$$I_{YX}(t)/F(t) = 1/9 - (2/9)\langle P_2\rangle + (1/9)G_{00}(t) - (1/3)G_{20}(t) \tag{4.38}$$

$$I_{XX}(t)/F(t) = 1/9 - (2/9)\langle P_2\rangle + (1/9)G_{00}(t) + (1/3)G_{20}(t) \tag{4.39}$$

Thus the time dependent polarization ratio is

$$r(t) = (\langle P_2\rangle + 2G_{00}(t))/(1 + 2\langle P_2\rangle) \tag{4.40}$$

for such a probe. The limiting value of $r(t)$ for long times is just

$$r(\infty) = \langle P_2 \rangle \tag{4.41}$$

since $G_{00}(\infty) = \langle P_2 \rangle^2$. The other limiting value is for $t = 0$. Using Table 2.3 we find

$$r(0) = \{2/5 + (11/7)\langle P_2 \rangle + (36/35)\langle P_4 \rangle\}/(1 + 2\langle P_2 \rangle) \tag{4.42}$$

Since $G_{00}(0) = \langle (P_2)^2 \rangle \geqslant \langle P_2 \rangle^2$ we have for a probe of this type $r(0) \geqslant r(\infty)$. The polarization ratio starts from a value depending on $\langle P_2 \rangle$ and $\langle P_4 \rangle$ and goes to a plateau value equal to $\langle P_2 \rangle$. Time dependent experiments on oriented systems can therefore give important information. From the plateau value $\langle P_2 \rangle$ can be extracted with its sign, thus allowing establishment of the average orientation of the probe. The order parameter $\langle P_4 \rangle$ is even more valuable since it cannot be easily obtained with other techniques [23]. The time dependence of $r(t)$ is, in this simple case, given by the long axis correlation function $G_{00}(t)$. An experimental decay if available can thus be simulated by assuming a strong collision or a diffusional model for the probe reorientation (cf. §2). A best fit to the experimental spectrum will give the motional parameters (correlation times or diffusion coefficients) implicit in these models.

In Fig. 4.2 we show the theoretical $r(t)$ curves predicted using the diffusion model for a DPH like probe subjected to the anisotropic potential Eqn. 2.17.

In the more general case that the absorption or emission dipole are tilted away from the axis of effective cylindrical symmetry other correlation functions apart from $G_{00}(t)$ may come in. This is shown more clearly if we

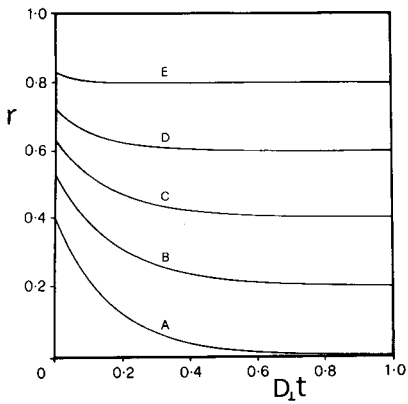

Fig. 4.2. The time-dependent polarization ratio $r(t)$ for an elongated probe with transition moments parallel to the long axis. The curves are calculated according to the diffusion model for $\langle P_2 \rangle$ equal to (A) 0.0, (B) 0.2, (C) 0.4, (D) 0.6, (E) 0.8.

transform the tensor components $A^{2,n}$, $\bar{A}^{2,n}$ from the molecule-fixed frame to their principal frames:

$$A^{2,n} = (2/3)^{1/2} D^2_{n0}(\Omega_{aM})^*$$

$$\bar{A}^{2,n} = (2/3)^{1/2} D^2_{n0}(\Omega_{eM})^*$$

where Ω_{aM}, Ω_{eM} are the orientations of the absorption and emission dipole, respectively, in the molecular frame. Due to the assumed cylindrical symmetry of the probe one of the dipoles, μ say, can always be taken to define the zx plane in the molecular frame. In this case $\Omega_{aM} = (0\beta_a 0)$, while $\Omega_{eM} = (\alpha_e \beta_e 0)$. Thus the dynamic terms $G_m(t)$ in Eqns. 4.25–4.30 can be written as (see Eqn. 4.16):

$$\sum_n G_{mn}(t) A^{2,n} \bar{A}^{2,n^*} = (2/3) \sum_n G_{mn}(t) D^2_{n0}(0\beta_a 0)^* D^2_{n0}(\alpha_e \beta_e 0) \qquad m = 0, \pm 2 \tag{4.43}$$

We see incidentally that only if at least one of the two transition moments is parallel to the molecular z axis it is possible to express results in terms of just the angle between the two dipoles. An exception is the case that the orientational correlation function $G_{mn}(t)$ does not depend on n. This is highly unrealistic in a liquid crystal as we discussed in §2. The importance of correctly placing the transition moment orientation in the molecular frame is well illustrated by the case of perylene. As we saw in §3, we may approximate perylene with a disk-like, or oblate ellipsoid, particle. While the emission transition dipole is parallel to the x axis (cf. Fig. 3.3), the absorption moment varies from being along the y axis when $\lambda_{ex} \sim 256$ nm to being itself parallel to x when $\lambda_{ex} \sim 430$ nm [82, 86]. The predicted decays vary quite dramatically in the two cases as shown in Figs. 4.3 and 4.4.

4.1.2. Steady state measurements

Although it seems in principle preferable to perform time dependent experiments whenever possible, fluorescence polarization measurements under continuous illumination conditions are much simpler and are routinely performed in very many laboratories. It is therefore interesting to examine what information these steady state experiments can offer. The fluorescence intensities are in this case time averages of Eqn. 4.2. For a certain geometry

$$I_{ij} = \int_0^\infty dt\, I_{ij}(t) \tag{4.44}$$

We shall assume for convenience that the fluorescence decay is mono-exponential i.e.

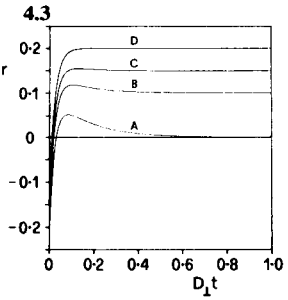

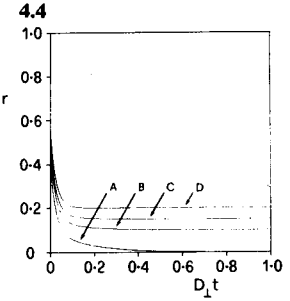

Fig. 4.3. Predicted polarization anisotropy $r(t)$ for an oblate ellipsoidal probe oriented in a monodomain when the absorption and emission transition moments are perpendicular to one another and to the disk axis (e.g. perylene at $\lambda_{ex} \sim 256$ nm). Diffusional reorientation with $D_{\parallel}/D_{\perp} = 10$ has been assumed. The disk axis order parameters are (A) 0.0, (B) −0.2, (C) −0.3, (D) −0.4.

Fig. 4.4. Theoretical polarization anisotropy decay $r(t)$ curves for a disk-like probe with transition moments along the x axis in a monodomain (e.g. perylene at $\lambda_{ex} \sim 430$ nm). The curves have been calculated according to the diffusion model, assuming $D_{\parallel}/D_{\perp} = 10$ and order parameters equal to (A) 0.0, (B) −0.2, (C) −0.3, (D) −0.4.

$$F(t) = \frac{1}{\tau_F} \exp(-t/\tau_F) \tag{4.45}$$

even though more complex forms can be considered with little effort.

General expressions for various geometries can be obtained from Eqns. 4.26–4.30 using one of the models seen earlier on for the correlation function.

We consider here the case of a cylindrically symmetric probe. To show the type of results obtained it is sufficient to consider the one exponential approximation, Eqn. 2.44, to the rotational diffusion correlation function $G_{mn}(t)$. We can calculate the steady state polarization index r_S,

$$r_S = (I_{ZZ} - I_{ZX})/(I_{ZZ} + 2I_{ZX}) \tag{4.46}$$

where

$$I_{ZZ} - I_{ZX} = \bar{A}^{2,0}\langle P_2\rangle/6^{1/2} + \sum_n A^{2,n}\bar{A}^{2,n^*}[G_{0n}(\infty) + (G_{0n}(0) - G_{0n}(\infty))\tau_{0n}/(\tau_{0n} + \tau_F)] \tag{4.47}$$

$$I_{ZZ} + 2I_{ZX} = (1/3) + (2/3)^{1/2}A^{2,0}\langle P_2\rangle \tag{4.48}$$

An equivalent expression is obtained for the strong collision model (cf. Eqn. 2.29).

In the special case that the emitting dipole is parallel to z, i.e. to the

molecular symmetry axis, while the absorption transition dipole makes an angle δ with z we have simply

$$I_{ZZ} - I_{ZX} = (1/3)\langle P_2\rangle + (2/3) \times \{\langle P_2\rangle^2 + [(1/5) + (2/7)\langle P_2\rangle + (18/35)\langle P_4\rangle - \langle P_2\rangle^2]\tau_{00}/(\tau_{00} + \tau_F)\}P_2(\cos\delta) \tag{4.49}$$

$$I_{ZZ} + 2I_{ZX} = (1/3) + (2/3)\langle P_2\rangle P_2(\cos\delta) \tag{4.50}$$

If, instead, the absorption transition moment is parallel to the molecular axis while the emitting dipole makes an angle δ with it we have

$$I_{ZZ} - I_{ZX} = \{(1/3)\langle P_2\rangle + (2/3) \times \{\langle P_2\rangle^2 + [1/5 + (2/7)\langle P_2\rangle + (18/35)\langle P_4\rangle - \langle P_2\rangle^2]\tau_{00}/(\tau_{00} + \tau_F)\}\}P_2(\cos\delta) \tag{4.51}$$

and

$$I_{ZZ} + 2I_{ZX} = 1/3 + (2/3)\langle P_2\rangle \tag{4.52}$$

Notice that a steady state experiment contains some limited information on dynamics in the form of correlation times τ_{mn} or rather of ratios τ_F/τ_{mn}. This information may prove rather difficult to extract since at every given temperature we have a number of unknowns (order parameters and correlation times) and only an experimental polarization value. The situation is worsened by the fact that changing the temperature all the parameters do in principle vary, including the fluorescence decay time τ_F.

4.2. Angular dependence experiments on monodomain samples

We wish to investigate here the possibility of studying the angular dependence of fluorescence polarization as a means of increasing the amount of experimental data, and thus allowing determination of order parameters [91]. This should be of importance in extracting $\langle P_2\rangle$ and even more so to obtain $\langle P_4\rangle$ when this determination is theoretically possible. The geometry of the experiment is only slightly different from the one considered in §4.1 and is shown in Fig. 4.5.

We consider a monodomain sample at the origin of the coordinate frame. Light linearly polarized along a unit vector $\mathbf{e}_i$ and propagating along the Y laboratory axis provides the required excitation of the fluorescent probe. The emitted light is observed along the incidence direction through a polarizer set at a direction $\mathbf{e}_f$. Typically the incident polarization direction is

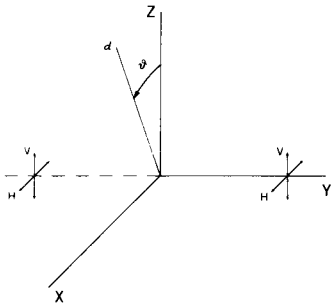

Fig. 4.5. Geometry of angular dependence experiment.

chosen along Z, while in emission both parallel ($I_{\parallel}$) and perpendicular ($I_{\perp}$) components are measured. Intensities are recorded as a function of the angle ϑ between the vertical and the sample director $\boldsymbol{d}$. The experimental set up used to actually perform the measurements depends on the type of sample we have at hand. For nematic liquid crystals a modified microscope has been used [94], where the aligned sample is rotated by using a rotating stage. In other situations, e.g. if the sample is aligned by flow [95], it might be convenient to simultaneously tilt the two polarizers in the excitation and emitted beam instead of actually rotating the sample. In any case director rotations are here restricted to the ZX plane. In other words for this experiment we consider rotating the monodomain about the direction of propagation of the exciting light (cf. Fig. 4.5). Thus

$$D^{L}_{mq}(d-L) = D^{L}_{mq}(0, \vartheta, 0) \tag{4.53a}$$

$$= d^{L}_{mq}(\vartheta) \tag{4.53b}$$

where $d^{L}_{mq}(\vartheta)$ is the usual notation for the small Wigner matrices defined in the Appendix [25]. We are now in a position to see explicitly what the predicted angular dependence for the experiment will be. To do this we first couple the two Wigner rotation matrices containing the angular dependence in Eqn. 4.10 using the Clebsch–Gordan series (Eqn. A12). The result is

$$I^{22}_{if}(t, \vartheta) = \sum (-)^{m'-q} E^{2,m*}_{i} E^{2,m'}_{f} C(22J; m-m') C(22J; q-q) \times$$
$$D^{2}_{m-m',0}(0, \vartheta, 0)^{*} G_{q}(t) \tag{4.54}$$

where $C(abc; de)$ is a Clebsch–Gordan coefficient [25]. The polarization tensor components have been given before in Eqns. 4.18–4.21. The intensities for various combinations of polarizer and analyzer can be obtained in explicit form. The algebra required for obtaining this is rather lengthy,

however, and the explicit expressions have been derived by performing the necessary algebraic manipulations on a computer, using the SCHOONSCHIP algebra system [96]. The resulting intensity expressions are relatively involved and will be reported elsewhere [91]. Here we show instead a rather illuminating limiting case for steady state measurements.

We assume as usual a single exponential decay for the intrinsic fluorescence decay (Eqn. 4.45) although the theory can be generalized to the case of more complex decays. We also consider the case of vertical excitation while observation is either vertical ($I_{\parallel}(\vartheta) = I_{ZZ}(\vartheta)$) or horizontal ($I_{\perp}(\vartheta) = I_{ZX}(\vartheta)$). The probe molecule is once more assumed to be rod-like, with transition moments parallel to the long axis, i.e. DPH-like. We adopt for the theoretical calculations both the diffusional model and the strong collision which we shall now consider in turn.

(*A*) *Diffusion model*: the first effect we wish to examine is that of the influence of the orientational order parameter $\langle P_2 \rangle$ on the fluorescence depolarization angular dependence pattern. Polar plots of our results are shown in Fig. 4.6a–c for three different values of the fluorescence to reorientational decay time ratio. Even though the general trend is similar, there are marked differences between the various cases. Thus, for example, if we choose low values of $\langle P_2 \rangle$, the $I_{\perp}$ curve lies inside the $I_{\parallel}$ curve for fluorescence decay times much shorter than reorientation time. On the other hand, this is not true if τ_F is somewhat larger than $D_{\perp}^{-1}$.

(*B*) *Strong collision model*: we now wish to investigate the effect that changing $\langle P_4 \rangle$ has on the fluorescence intensities pattern. To this end the so-called strong collision model is most conveniently used. In this case we do not have to assume an anisotropic pseudopotential acting on the molecule to start with since $\langle P_4 \rangle$ appears as an empirical adjustable parameter. The orientational correlation functions in the strong collision model are assumed to be single exponentials (cf. Eqn. 2.29). In this model every spherical component of the transition tensor is assumed to decay with its own time τ_n. These orientational decay times are empirical parameters to be determined. The model is therefore particularly convenient when only one or two correlation times are needed, as is the case when both transition moments are either parallel or perpendicular to the long axis. We have then considered a certain value of the order parameter $\langle P_2 \rangle$ and of the ratio of fluorescence to reorientation time, and from these we have computed the intensity patterns for various values of $\langle P_4 \rangle$. These results are shown in Fig. 4.7a–d.

Here we notice first of all that, if $\tau_F > \tau_0$ (Fig. 4.7a), the effect of varying $\langle P_4 \rangle$ on the curves is very limited. According to our results a value of $\tau_F \geqslant 2\tau_0$ is sufficient to make the experiment very insensitive to $\langle P_4 \rangle$. This in turn means that attempts to determining $\langle P_4 \rangle$ from fluorescence depolarization angular dependence experiments (and even more so from normal steady

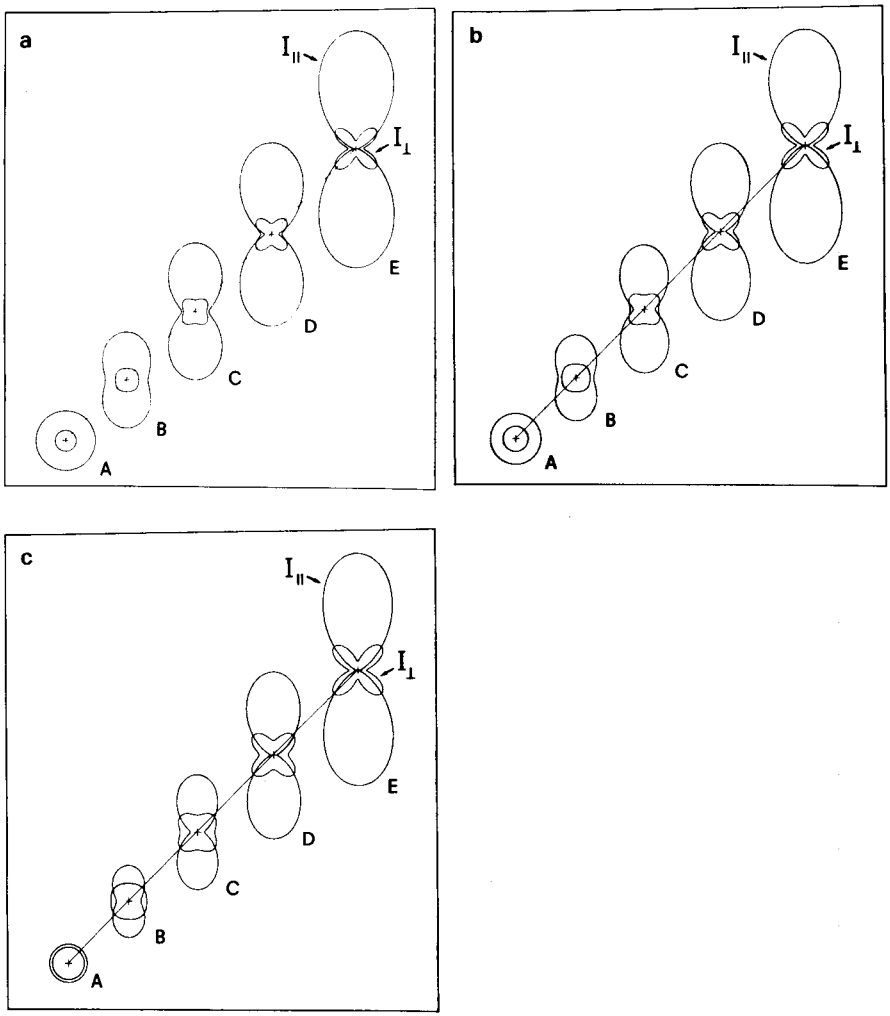

Fig. 4.6. The effect on the angular dependent fluorescence intensities $I_{\parallel}(\vartheta)$, $I_{\perp}(\vartheta)$ of varying the order parameter $\langle P_2 \rangle$. A DPH like probe with transition moments parallel to the long axis is considered. $\langle P_2 \rangle$ takes the values (A) 0.0, (B) 0.2, (C) 0.4, (D) 0.6, (E) 0.8. The three sets of polar plots illustrate various ratios of fluorescence to reorientational decay times: (a) $\tau_F = 0.01 D_{\perp}^{-1}$; (b) $\tau_F = 0.1 D_{\perp}^{-1}$; (c) $\tau_F = D_{\perp}^{-1}$.

state experiments) are not likely to be successful or accurate. As we shall see later on this has often been overlooked in the past.

A more interesting situation arises when $\tau_F < \tau_0$. In this case the theoretical angular patterns are rather sensitive to the fourth rank order parameter. In particular when $\langle P_4 \rangle$ goes from positive to negative values the pattern

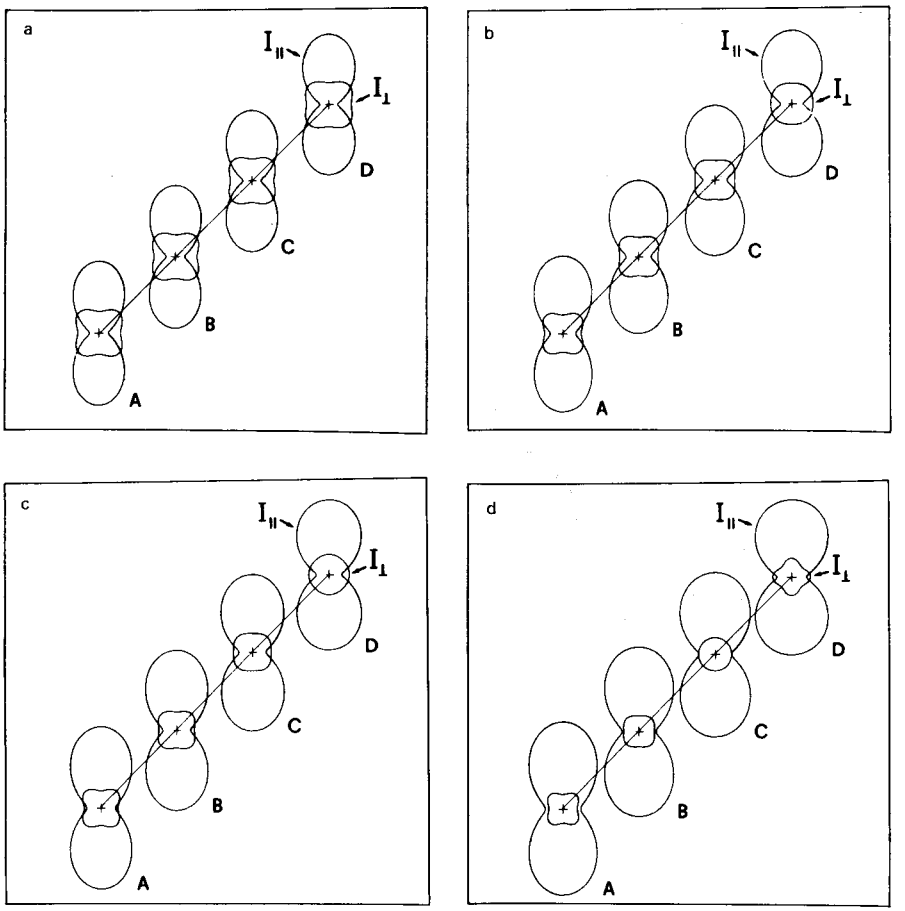

Fig. 4.7. The effect of changing the order parameter $\langle P_4 \rangle$ on the angular dependent fluorescence intensities $I_{\parallel}(\vartheta)$, $I_{\perp}(\vartheta)$ for a DPH like probe according to the strong collision model. Here we keep the order parameter $\langle P_2 \rangle$ fixed at 0.4 and consider four values of $\langle P_4 \rangle$: (A) 0.1041 (Mean Field value); (B) 0.05; (C) 0.00; (D) −0.1. Each set of polar patterns corresponds to a certain ratio of fluorescence to reorientation decay time τ_F/τ_0: (a) 5.0; (b) 1.0; (c) 0.5; (d) 0.01.

changes from a four leaf to a cross shaped type. This is particularly apparent when $\tau_F \ll \tau_0$, as shown in Fig. 4.7d. In this limit we have, in particular, that the $I_{\perp}$ pattern becomes a circle when $\langle P_4 \rangle = 0$. Using again a procedure written in SCHOONSCHIP we can obtain explicit results for the intensities. We find

$$I_{\parallel}(\vartheta) = 1/5 + (-2/7 + 6\cos^2\vartheta/7)\,\langle P_2 \rangle + (3/35 - 6\cos^2\vartheta/7 + \cos^4\vartheta)\langle P_4 \rangle \tag{4.55a}$$

$$I_{\perp}(\vartheta) = 1/15 + (1/21)\langle P_2\rangle + (-4/35 + \cos^2\vartheta - \cos^4\vartheta)\langle P_4\rangle \tag{4.55b}$$

These equations show quite neatly that indeed the $I_{\perp}$ pattern becomes a circle when $\langle P_4\rangle = 0$. It is also easy to see how the pattern changes symmetrically with respect to the circle, when $\langle P_4\rangle$ changes sign. In this case the same numerical quantity is either added to or subtracted from the circle. Needless to say this simple equation only holds when $\tau_F \ll \tau_0$. On the other hand it is in this limit that the experiment is most sensitive to $\langle P_4\rangle$. This limit could be achieved in practice using either probes with sub-nanosecond decay time or rather viscous liquid crystals.

Another angular dependent experiment has been recently considered by Kooyman et al. [92]. They considered homotropically aligned samples, with the director perpendicular to the sample cell glass slides. In view of the geometrical constraint on the director they chose to perform excitation with radiation propagating at an angle ψ to the bilayer normal. They then performed an angular dependent study by varying this angle of incidence. Their experimental set up will be particularly useful for studies on oriented bilayers.

4.3. Macroscopically isotropic systems

We now turn to the case, especially relevant in biophysics [97–99] of experiments performed on vesicles [7b, 8–19]. We first derive general model independent equations for $r(t)$ valid even for a non-cylindrically symmetric probe. We shall then discuss the time-dependence expected for a cylindrically symmetric probe reorienting according to one of the models previously examined i.e. the diffusion and the strong collision model [19].

4.3.1. General relations

We start once more from Eqn. 4.10 or rather from a slight generalization of this where we relax the assumption that the director is fixed in space. Thus we have for the rank L, L' contribution to the total intensity

$$I_{if}^{LL'}(t) = \sum E_i^{L,m^*} E_f^{L',m'} A^{L,n} \bar{A}^{L',n'^*} \langle\langle D_{mq}^{L}(d_0 - L)^* D_{m'q'}^{L'}(d_t - L) D_{qn}^{L}(0 - d_0)^* D_{q'n'}^{L'}(t - d_t)\rangle\rangle \tag{4.56}$$

where the double angular brackets indicate an average over the local director motion with respect to the laboratory frame and over the molecular reorientation with respect to the director. For a vesicle we can assume these

two motions to be uncoupled, i.e.

$$\langle\langle D^{L}_{mq}(d_0 - L)^* D^{L'}_{m'q'}(d_t - L) D^{L}_{qn}(0 - d_0)^* D^{L'}_{q'n'}(t - d_t)\rangle\rangle$$
$$= \langle D^{L}_{mq}(d_0 - L)^* D^{L'}_{m'q'}(d_t - L)\rangle_d \langle D^{L}_{qn}(0 - d)^* D^{L'}_{q'n'}(t - d)\rangle \tag{4.57}$$

where $\langle \ldots \rangle_d$ indicates an average over the local director motions and $\langle \ldots \rangle$ an average over molecular reorientation with respect to the director; we have removed the unnecessary subscripts in this last term. Here the local director time-dependence in the laboratory frame is given by the overall vesicle reorientation. For an ordinary vesicle with a diameter of a few thousand nanometers, the overall tumbling time will be orders of magnitude longer than the fluorescence decay time. Therefore we can safely assume at this stage the director distribution to be static on the experimental time scale. Due to macroscopic spherical symmetry this distribution will be isotropic and we can write the average over the distribution of directors as

$$\langle D^{L}_{mq}(d - L)^* D^{L'}_{m'q'}(d - L)\rangle_d = \delta_{LL'}\delta_{mm'}\delta_{qq'}/(2L + 1) \tag{4.58}$$

by exploiting the orthogonality of the Wigner rotation matrices (Eqn. A7). After the macroscopic average has been taken we are left with only two surviving components i.e.

$$I^{0,0}_{if} = \tfrac{1}{9} \tag{4.59a}$$

and

$$I^{2,2}_{if} = \tfrac{1}{5} \sum E^{2,m}_{i} E^{2,m^*}_{f} G(t) \tag{4.59b}$$

where

$$G(t) = \sum \langle D^{2}_{qn}(0 - d)^* D^{2}_{qn'}(t - d)\rangle A^{2,n} \bar{A}^{2,n'^*} = \sum G_q(t) \tag{4.60}$$

and we have not yet made any assumption about the probe symmetry.

We see from Eqns. 4.5 and 4.59 that the geometrical information about the experiment is all contained in the product $E^{2,m}_{i} E^{2,m^*}_{f}$, while $G(t)$ contains all the molecular information. The various experimental geometries discussed in §4.1 are here all equivalent in principle. We find in fact

$$I_{\parallel}(t) \equiv I_{ZZ}(t) = I_{XX}(t) = I_{YY}(t)$$
$$= \tfrac{1}{9} + \tfrac{2}{15} G(t) \tag{4.61}$$

and

$$I_{\perp}(t) \equiv I_{ZX}(t) = I_{ZY}(t) = I_{XY}(t)$$
$$= \tfrac{1}{9} - \tfrac{1}{15} G(t) \tag{4.62}$$

with $I_{if}(t) = I_{fi}(t)$. We obtain therefore the time-dependent polarization ratio as

$$r(t) = (I_{\parallel}(t) - I_{\perp}(t))/(I_{\parallel}(t) + 2I_{\perp}(t)) \tag{4.63}$$
$$= \tfrac{3}{5} G(t) \tag{4.64}$$

Equation 4.64, together with the definitions 4.16, 4.60, constitutes a general expression for $r(t)$ as a sum of orientational correlation functions $\langle D^2_{qn}(0-d)^* D^2_{qn'}(t-d)\rangle$. Another, perhaps more illuminating, expression can be obtained from Eqn. 4.60 by changing the sense of the first rotation through the relation $D^L_{qn}(0-d)^* = D^L_{nq}(d-0)$ and subsequently employing the closure relation of the Wigner matrices (Eqn. A10) in the form

$$\sum_q D^L_{nq}(d-0) D^L_{qn'}(t-d) = D^L_{nn'}(t-0) \tag{4.65}$$

We can in this way evaluate the sum over q to obtain

$$r(t) = \tfrac{3}{5} \sum \langle D^2_{nn'}(t-0)\rangle A^{2,n} \bar{A}^{2,n'*} \tag{4.66}$$

Thus the polarization ratio depends only on the relative orientation correlation function $\langle D_{nn'}(t-0)\rangle$. While the detailed form of the time-dependence will be discussed later, we now wish to obtain some general results for the short time and long time limiting values of $r(t)$. From Eqn. 4.66 we find the initial value of the polarization ratio as:

$$r(0) = \tfrac{3}{5} \sum \delta_{nn'} A^{2,n} \bar{A}^{2,n'*}$$
$$= \tfrac{2}{5} P_2(\cos \beta_{ae}) \tag{4.67}$$

where β_{ae} is the angle between the absorption and emission transition dipoles. To go from Eqn. 4.66 to Eqn. 4.67 we have used the fact that the rotation at time $t = 0$ is $D^2_{nn'}(0-0) = \delta_{nn'}$ and the explicit expression for the **A**, $\bar{\mathbf{A}}$ tensors spherical components (cf. Table A1). The result in Eqn. 4.67

holds for molecules of arbitrary shape. The limiting plateau value of $r(t)$ for very long times can also be written down explicitly as

$$r(\infty) = \tfrac{3}{5}\Big(\sum \langle D^{2*}_{qn}\rangle A^{2,n}\Big)\Big(\sum \langle D^{2}_{qn'}\rangle \bar{A}^{2,n'*}\Big) \tag{4.68}$$

where $\langle D^2_{qn}\rangle$ is an order parameter for the probe as introduced in §2. Notice that the equations given for $r(t)$ and its boundary values are quite general as up to this stage no assumption has been made about the symmetry of the local environment or of the probe. Since we find that the initial value $r(0)$ is a constant, it follows that it cannot give any information on these symmetries. The long time limit is more informative and the general expression in Eqn. 4.68 adopts simpler forms if some symmetry exists, since this reflects on the order parameters $\langle D^2_{qn}\rangle$ (cf. §2). Particularly important is the case of local uniaxial symmetry. In this instance a rotation around the local director cannot have any effect so that we must have

$$\langle D^2_{qn}\rangle = \delta_{q0}\langle D^2_{0n}\rangle \tag{4.69}$$

and long time value of the polarization anisotropy i.e. the plateau reduces to

$$r(\infty) = \tfrac{3}{5}\,\tilde{A}^{2,0}\bar{\tilde{A}}^{2,0*} \tag{4.70}$$

where the upper tilde denotes the partially averaged components familiar in magnetic resonance studies [20], i.e.

$$\tilde{A}^{2,0} = \sum \langle D^{2*}_{0n}\rangle A^{2,n} \tag{4.71}$$

Further simplifications require examining the probe symmetry as well. We consider as an example biaxial molecules with point symmetry D_{2h} analogous to that of the popular fluorescent probes anthracene and tetracene. It was shown in Ref. 23 that for D_{2h} molecular symmetry the order parameter $\langle D^2_{0,n}\rangle$ can be different from zero only for $n = 0, \pm 2$ and that $\langle D^2_{0,2}\rangle = \langle D^2_{0,-2}\rangle$. Thus for these lathe-like probes we find the plateau value of the polarization ratio to be

$$r(\infty) = \tfrac{3}{5}\,A^{2,0}\langle P_2\rangle + (2\,Re\,A^{2,2})\langle D^2_{02}\rangle\bar{A}^{2,0}\langle P_2\rangle + (2\,Re\,\bar{A}^{2,2})\langle D^2_{02}\rangle \tag{4.72}$$

where the usual notation $\langle P_2\rangle$ has been used for $\langle D^2_{00}\rangle$. The order parameter

$\langle D^2_{02}\rangle$ is a measure of the deviation from molecular cylindrical symmetry. As discussed in §2.1.1 it has been treated theoretically using mean field theory [32] and is currently measured by other physical techniques, for example, NMR [42] and ESR [100]. The information obtained in a certain experiment depends on the orientation of the absorption and emission dipoles in the molecular system, chosen as usual as the principal axis system for the ordering tensor and with the z axis as the axis of greatest symmetry. Results for various transition moments orientations for biaxial particles are given in Table 4.2.

Let us now examine the case of a probe with a cylindrically symmetric ordering matrix. In this instance we find [23] $\langle D^2_{qn}\rangle = \delta_{q0}\delta_{n0}\langle P_2\rangle$. From Eqn. 4.68 we obtain the long-time limit as

$$r(\infty) = \tfrac{3}{5} A^{2,0}\bar{A}^{2,0^*}\langle P_2\rangle^2 \tag{4.73}$$

By transforming the absorption and emission tensors to their principal frames we can rewrite Eqn. 4.73 as

$$r(\infty) = \tfrac{2}{5} P_2(\cos\beta_a)P_2(\cos\beta_e)\langle P_2\rangle^2 \tag{4.74}$$

a result also obtained by Lipari and Szabo [17]. This is the limiting value of the polarization for a probe with cylindrically symmetric ordering tensor and absorption and emission moments at angles β_a, β_e respectively, from the cylindrical symmetry axis $\boldsymbol{l}$. For a rod-like probe with $\boldsymbol{\mu}\|\bar{\boldsymbol{\mu}}\|\boldsymbol{l}$ such as an idealized DPH [9]

$$r(\infty) = \tfrac{2}{5}\langle P_2\rangle^2 \tag{4.75}$$

Notice that this plateau value contains information on the second rank order parameter $\langle P_2\rangle$ as in the monodomain case (§4.1.1). Here however $\langle P_2\rangle$ is squared and the information about its sign is lost. This might make it more

TABLE 4.2

LONG TIME LIMITING VALUES OF THE FLUORESCENCE DEPOLARIZATION FOR BIAXIAL PROBES [19]

Results are given for various values of the absorption ($\boldsymbol{\mu}$) and emission ($\bar{\boldsymbol{\mu}}$) transition moments in the molecular frame in terms of the order parameters $\langle D^2_{00}\rangle$, $\langle D^2_{02}\rangle$.

Configuration	$r(\infty)$
$\boldsymbol{\mu}\|\bar{\boldsymbol{\mu}}\|z$	$(2/5)\langle P_2\rangle^2$
$\boldsymbol{\mu}\|z, \bar{\boldsymbol{\mu}}\|x$	$-(1/5)\langle P_2\rangle\{\langle P_2\rangle - 6^{1/2}\langle D^2_{02}\rangle\}$
$\boldsymbol{\mu}\|x, \bar{\boldsymbol{\mu}}\|y$	$(3/5)\{(1/6)\langle P_2\rangle^2 - \langle D^2_{02}\rangle\}$
$\boldsymbol{\mu}\|\bar{\boldsymbol{\mu}}\|x$	$(1/10)\{\langle P_2\rangle^2 - 2(6)^{1/2}\langle P_2\rangle\langle D^2_{02}\rangle + 6\langle D^2_{02}\rangle^2\}$

difficult to establish if the average orientation of a certain probe is parallel or perpendicular to the bilayer normal (§2.1).

For molecules with $\boldsymbol{\mu} \| \bar{\boldsymbol{\mu}} \perp \boldsymbol{l}$ or $\boldsymbol{\mu} \perp \bar{\boldsymbol{\mu}} \perp \boldsymbol{l}$ such as perylene and other aromatic hydrocarbons we have instead

$$r(\infty) = \tfrac{1}{10} \langle P_2 \rangle^2 \tag{4.76}$$

Our results for these two simple limiting cases agree with those published in Ref. 9. However, even for the simplest case of cylindrical symmetry Eqn. 4.74 is more general than those given by Kinosita et al. [9]. In particular it is interesting to note that in the long time limit the angles β_a, β_e between the molecular axis [101] and each transition moment have to be known, and not just the relative angle β_{ae} between them as in the short time limit. Thus, for example, if at least one of the two transition dipoles is at the so-called magic angle, $\beta = \arccos(1/3^{1/2}) \sim 54.7°$, the angular term in Eqn. 4.74 vanishes and the limiting value of the fluorescence polarization is predicted to be zero. If, instead, the order parameter $\langle P_2 \rangle$ is known from some independent measurement, information on the transition moments orientation in the molecular frame can be gathered. This geometrical dependence might be of help for example in locating the orientation of a chromophore attached to a macromolecule. Alternatively it could be used to obtain insight into the disposition of a certain intrinsic chromophore in a protein.

4.3.2. Dynamic effects

We shall examine in detail the case of a probe with effective cylindrical symmetry. In this instance we can apply (cf. §2) the following symmetry restriction on the orientational correlation functions

$$\begin{aligned} \langle D^2_{qn}(0-d)^* D^2_{qn'}(t-d) \rangle &= \delta_{nn'} \langle D^2_{qn}(0-d)^* D^2_{qn}(t-d) \rangle \\ &= \delta_{nn'} G_{qn}(t) \end{aligned} \tag{4.77}$$

Thus we find from Eqns. 4.60 and 4.64

$$r(t) = \tfrac{3}{5} \sum_n A^{2,n} \bar{A}^{2,n^*} \sum_q G_{qn}(t) \tag{4.78a}$$

$$= \tfrac{3}{5} \sum_n A^{2,n} \bar{A}^{2,n^*} \langle D^2_{nn}(t-0) \rangle \tag{4.78b}$$

The time evolution of the polarization ratio is therefore given by the sum of orientational correlation functions. The information content and physical significance will be tackled systematically later on. Here we wish to discuss the calculation of $r(t)$ and make some comparison between the polarization decay

in a monodomain sample [4] and in a membrane vesicle. We consider the usual example of an elongated probe with transition moments parallel to the long axis. We have seen earlier that

$$r(t) = \{\langle P_2\rangle + 2G_{00}(t)\}/(1 + 2\langle P_2\rangle) \tag{4.79}$$

for a monodomain sample. Hence at least in principle, the Wigner correlation function $G_{00}(t)$ can be extracted from the time decay. A similar experiment performed on a vesicle suspension would give instead

$$r(t) = \tfrac{2}{5}\langle D^2_{00}(t-0)\rangle \tag{4.80}$$

which is just a sum of orientational correlation functions as shown by Eqn. 4.78a. By employing the symmetry relations (Eqn. 2.25) valid for cylindrically symmetric probes and mesophases, we can write for a DPH-like probe

$$r(t) = \tfrac{2}{5}\{G_{00}(t) + 2G_{10}(t) + 2G_{20}(t)\} \tag{4.81}$$

The Wigner matrix correlation functions in Eqn. 4.78a are of course those for a molecule reorienting in an anisotropic environment [4]. They can be calculated using a specific reorientation model. We consider, as in the previous sections, two cases.

(*a*) *Diffusion model*: in Fig. 4.8 we show, as an illustration, results for the time-dependence of $r(t)$ obtained using a Maier-Saupe-like truncation (Eqn. 2.17). We note that the theoretical predictions are in excellent agreement with the recent experimental findings of a number of authors [9, 10, 13–18] using the DPH probe which very closely mimicks the idealized case of an effectively cylindrically symmetric molecule with absorption and emission moments parallel to the long axis.

Notice that, as shown earlier, there is a limiting value $r(\infty) \neq 0$ as soon as the local order parameter $\langle P_2\rangle \neq 0$. The true isotropic medium condition is obtained for $\langle P_2\rangle = 0$. In this limit the standard isotropic results [2] are recovered. The diffusion model gives

$$r(t) = \tfrac{2}{5}\exp(-6D_\perp t) \tag{4.82}$$

in the isotropic limit, with $D_\perp$ being the perpendicular component of the rotational diffusion tensor. According to the diffusion model, the decay of $r(t)$ is not a simple exponential in an ordered system i.e. when $\langle P_2\rangle \neq 0$ even when $\boldsymbol{\mu}$, $\bar{\boldsymbol{\mu}}$ are along the symmetry axis. This is perhaps most apparent if we consider the approximate one exponential form of the Wigner correlation $G_{mn}(t)$ which holds for degrees of order which are not too high (Eqn. 2.44). Within this approximation we find

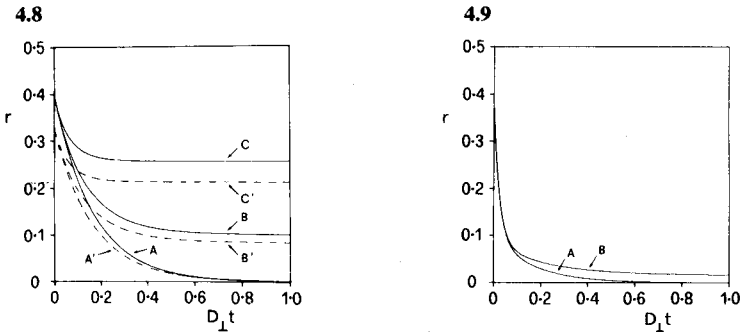

Fig. 4.8. The time-dependent polarization ratio $r(t)$ for an elongated cylindrically symmetric probe. Solid curve for absorption and emission dipole moments parallel to the molecular axis, dashed curve for transition moments tilted 20° off axis. Curves calculated according to the diffusion model for $\langle P_2 \rangle$ equal to (A, A') 0.0, (B, B') 0.5, (C, C') 0.8.

Fig. 4.9. Theoretical $r(t)$ for a perylene type probe in a vesicle calculated according to the diffusion model of reorientation (potential Eqn. 2.17). Here $\boldsymbol{\mu} \| \bar{\boldsymbol{\mu}} \perp \mathbf{z}$ (cf. Fig. 3.3). The local order parameter $\langle P_2 \rangle$ is respectively (A) 0.0, (B) −0.4.

$$\sum_q G_{qn}(t) = \sum_q G_{qn}(0) \exp(-t/\tau_{qn}) - \delta_{n0}\langle P_2 \rangle^2 \exp(-t/\tau_{00}) + \langle P_2 \rangle^2 \delta_{n0} \tag{4.83}$$

which when substituted in Eqn. 4.78a yields

$$r(t) = \tfrac{3}{5} \sum A^{2,n} \bar{A}^{2,n*} \{ [G_{qn}(0) - \delta_{q0}\delta_{n0}\langle P_2 \rangle^2] \exp(-t/\tau_{qn}) + \langle P_2 \rangle^2 \delta_{n0} \} \tag{4.84}$$

where the explicit values of the correlation function initial values $G_{qn}(0)$ have been given previously in terms of order parameters $\langle P_2 \rangle$ and $\langle P_4 \rangle$ (cf. Table 2.3). We can see that even if the transition moments are parallel to the cylinder axis, i.e. if $n = 0$ in Eqn. 4.84, a sum of three exponentials is obtained. The dynamic information is contained, in general, in the correlation times τ_{qn}. In the diffusion model these time constants all follow from the only dynamic input parameters for the calculation, i.e. from the diffusion tensor components $D_\parallel$, $D_\perp$. As is apparent from the structure of the diffusion matrix (Eqn. 2.38) no information on the ratio $D_\parallel / D_\perp$ can be obtained if both the absorption and emission moment are parallel to the molecular symmetry axis. The predicted decay appears as a sum of three exponentials. However it would be dangerous to use an unconstrained three exponential fitting procedure for an experimental curve since the three pre-exponential factors and the three correlation times τ_{q0} are not independent.

After substitution for $G_{qn}(0)$ we have the explicit expression

$$r(t) = (2/5)\{1/5 + (2/7)\langle P_2\rangle + (18/35)\langle P_4\rangle - \langle P_2\rangle^2\} \exp(-t/\tau_{00}) + \langle P_2\rangle^2$$
$$+ (2/5)\{1/5 + (1/7)\langle P_2\rangle - (12/35)\langle P_4\rangle\} \exp(-t/\tau_{10})$$
$$+ (2/5)\{1/5 - (2/7)\langle P_2\rangle + (3/35)\langle P_4\rangle\} \exp(-t/\tau_{20}) \qquad (4.85)$$

The parameters of the three exponentials are obtained simultaneously from the solution of the diffusion equation when a model potential and a value for $D_\perp$ are assumed. Thus if the Maier-Saupe-like potential (Eqn. 2.17) is considered, the only independent parameters are $\langle P_2\rangle$ and $D_\perp$. The value of $\langle P_4\rangle$ can be read off from Fig. 2.5 and the three correlation times τ_{00}, τ_{10}, τ_{20} are plotted in Ref. 50 as a function of $\langle P_2\rangle$. As a practical consequence the best way of analyzing experimental data is not to perform a fit to a sum of exponentials but rather to choose a model potential and fit the hopefully smaller number of parameters that the model involves. The decay curves for $r(t)$ are modified if the transition moments are tilted away from the symmetry axis. As an illustration we show (dashed curve in Fig. 4.8) the effect of a tilt of 20° for a DPH-like probe. Notice also that the steepness of the decay depends on $D_\parallel/D_\perp$ when the transition moments are off axis [19].

We now examine once more the case of a perylene-type probe. Consider $\lambda_{ex} \sim 430$ nm so that $\boldsymbol{\mu} \| \bar{\boldsymbol{\mu}} \perp \mathbf{z}$. Working through some algebra we get from Eqn. 4.78a the model independent expression

$$r(t) = \tfrac{3}{5}\{\tfrac{1}{6} G_{00}(t) + \tfrac{1}{3}[G_{10}(t) + G_{20}(t)] + \tfrac{1}{2} G_{02}(t) + G_{12}(t) + G_{22}(t)\} \qquad (4.86)$$

We have evaluated this $r(t)$ using the diffusion model, as before, obtaining the curves shown in Fig. 4.9. The other limiting geometry for the transition moments i.e. $\boldsymbol{\mu} \| \mathbf{y}$, $\bar{\boldsymbol{\mu}} \| \mathbf{x}$ (cf. Fig. 3.3) yields

$$r(t) = \tfrac{3}{5}\{\tfrac{1}{6} G_{00}(t) + \tfrac{1}{3}[G_{10}(t) + G_{20}(t)] - \tfrac{1}{2} G_{02}(t) - G_{12}(t) - G_{22}(t)\} \qquad (4.87)$$

with

$$r(\infty) = \tfrac{1}{10}\langle P_2\rangle^2$$

the same limiting value holding also for Eqn. 4.86.

Substituting the diffusional correlation functions gives the peculiar looking pattern in Fig. 4.10.

Notice that similar curves with a negative starting polarization have been obtained experimentally by e.g. Brand et al. [84], for $\lambda_{ex} \sim 256$ nm. According to our theoretical curves perylene does not seem to be a very sensitive probe for local ordering in vesicles. Both configurations of transition

4.10

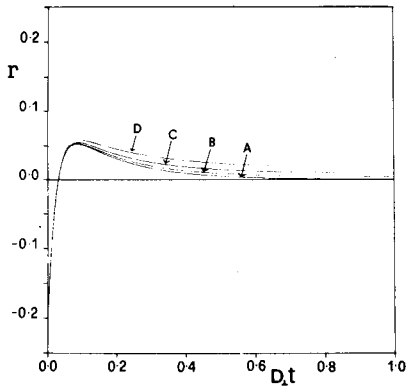

4.11

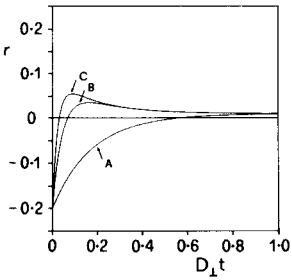

Fig. 4.10. Predicted polarization anisotropy time variation $r(t)$ for a perylene type probe with $\mu \| y$, $\bar{\mu} \| x$ (cf. Fig. 3.3) in a vesicle. Simulation performed using the diffusional reorientation model with potential Eqn. 2.17 and $D_\parallel/D_\perp = 10$. The various curves correspond to a local order $\langle P_2 \rangle$ of (A) 0.0, (B) −0.2, (C) −0.3, (D) −0.4.

Fig. 4.11. The effect of varying the rotational diffusion tensor anisotropy $D_\parallel/D_\perp$ for a perylene type probe with $\mu \| y$, $\bar{\mu} \| x$ in a vesicle. Here $\langle P_2 \rangle = -0.3$ and $D_\parallel/D_\perp$ is (A) 1, (B) 5, (C) 10.

moments yield very similar curves as $\langle P_2 \rangle$ goes from its isotropic value to −0.4 (close to the limiting value of −0.5).

Perylene seems to be more sensitive on the other hand to variations in the rotational anisotropy. We show in Fig. 4.11 the effect of varying $D_\parallel/D_\perp$ from 1 to 10 for a local $\langle P_2 \rangle = -0.3$. Essentially the same pattern is obtained for an isotropic solvent ($\langle P_2 \rangle = 0$).

(*b*) *Strong collision model*: a very simple and compact expression for the polarization ratio can be obtained if the strong collision expression (Eqn. 2.29) for the correlation functions $G_{qn}(t)$ is used in Eqn. 4.78. In this instance, since the correlation times τ_{qn} are assumed to depend only on n, the sum upon q can be performed explicitly to give

$$\sum_q G_{qn}(t) = (1 - \langle P_2 \rangle^2 \delta_{n0}) \exp(-t/\tau_n) + \langle P_2 \rangle^2 \delta_{n0} \tag{4.88}$$

Hence, for an arbitrary orientation of the transition moments specified by their components $A^{2,n}\bar{A}^{2,n}$, the strong collision expression for the polarization decay is

$$r(t) = \tfrac{3}{5}\left\{ \sum_n A^{2,n}\bar{A}^{2,n*}(1 - \langle P_2 \rangle^2 \delta_{n0}) \exp(-t/\tau_n) + A^{2,0}\bar{A}^{2,0*}\langle P_2 \rangle^2 \right\} \tag{4.89}$$

In this simple model we recall that each spherical tensor component

reorients with its own time constant τ_n. The physical significance of τ_0 is that of a correlation time relative to reorientation of the molecular z axis. If this motion takes place much more slowly than that of the x and y axis, the correlation time τ_2 relates essentially to reorientation about the molecular symmetry axis (cf. Fig. 2.7). Here the expressions for $r(t)$ are simpler than the diffusional ones, but each different correlation time has to be considered an independent parameter.

4.3.3. Continuous illumination experiments

As mentioned in §4.1.2 expressions for steady state intensities can be obtained by integrating the corresponding time-dependent quantities (cf. Eqn. 4.44). We find in general for cylindrically symmetric probes and local uniaxial symmetry the depolarization ratio r_s, as

$$r_s = (I_\parallel - I_\perp)/(I_\parallel + 2I_\perp) \tag{4.90}$$

thus

$$r_s = \tfrac{3}{5} \sum_n A^{2,n} \bar{A}^{2,n^*} \sum_q \int G_{qn}(t) \exp(-t/\tau_F)\, dt/\tau_F \tag{4.91}$$

which can be readily calculated for the two reorientation models considered in §2.2.

(*a*) *Diffusion model*: using the expansion for $G_{qn}(t)$ as a sum of exponentials given in Eqn. 2.41 we find

$$r_s = \tfrac{3}{5} \sum_n A^{2,n} \bar{A}^{2,n^*} \sum (b^{qn})_K \tau_{qn}^K/(\tau_{qn}^K + \tau_F) \tag{4.92}$$

The expression can be simplified by retaining only the first terms of Eqn. 2.41. However, a simpler expression can be obtained using the strong collision model.

(*b*) *Strong collision model*: here we make use of Eqn. 4.88 to obtain

$$r_s = \tfrac{3}{5} A^{2,0} \bar{A}^{2,0^*} \langle P_2 \rangle^2 + \tfrac{3}{5} \sum_n A^{2,n} \bar{A}^{2,n^*} (1 - \langle P_2 \rangle^2 \delta_{n0}) \tau_n/(\tau_n + \tau_F) \tag{4.93}$$

This very simple equation holds for any orientation of the transition moments in the molecular frame. It generalizes and shows the limit of validity of similar expressions previously obtained by other authors [14, 15], to which it reduces when $\boldsymbol{\mu} \| \bar{\boldsymbol{\mu}} \| \boldsymbol{l}$

$$r_s = \tfrac{2}{5} \langle P_2 \rangle^2 + \tfrac{2}{5} (1 - \langle P_2 \rangle^2) \tau_0/(\tau_0 + \tau_F) \tag{4.94}$$

In this special case, only the correlation time τ_0 relative to long axis reorientation appears. For an elongated probe $\langle P_2 \rangle$ is positive and should decrease with temperature so the polarization ratio is expected to decrease with temperature. This is not necessarily the case if at least one of the transition moments is off-axis. For instance if the absorption moment makes an angle β_a with the long axis (and the emission moment)

$$r_s = \tfrac{2}{5} P_2(\cos \beta_a)\langle P_2 \rangle^2 + \tfrac{2}{5} P_2(\cos \beta_a)(1 - \langle P_2 \rangle^2)\tau_0/(\tau_0 + \tau_F) \tag{4.95}$$

If the angle β_a is greater than the magic angle, the polarization ratio will be negative and will tend to zero from below as the temperature increases. Notice that to observe more than one correlation time, and in particular the correlation time τ_2 related mainly to reorientation about the long axis, a probe with both moments off-axis is needed. For example, if both μ, $\bar{\mu}$ are perpendicular to the long axis and $\boldsymbol{\mu} \| \bar{\boldsymbol{\mu}}$

$$r_s = \tfrac{1}{10}\langle P_2 \rangle^2 + \tfrac{3}{10}\left\{\tfrac{1}{3}(1 - \langle P_2 \rangle^2)\frac{\tau_0}{\tau_0 + \tau_F} + \frac{\tau_2}{\tau_2 + \tau_F}\right\} \tag{4.96}$$

For an elongated molecule it is expected that $\tau_2 < \tau_0$ [19] and it should be possible to estimate the importance of the term containing τ_2. In any case, the relative importance of the two contributions depends on the order. In the limiting case of complete local order, $\langle P_2 \rangle = 1$, only the τ_2 second term in Eqn. 4.96 survives and

$$r_s = \tfrac{1}{10} + \tfrac{3}{10}\frac{\tau_2}{\tau_2 + \tau_F} \tag{4.97}$$

In physical terms this means that when the local order is complete, only modulation of the fluorescence due to reorientation about the long axis is possible. As we see there are a variety of expressions obtained for the polarization anisotropy as the transition moments geometry varies. It is most important that this is taken into account when analyzing experimental data.

5. Applications of fluorescence depolarization studies to membranes

There have been a great number of applications of the fluorescent probe technique to the investigation of order and fluidity in model and real membranes [7–17, 28–30, 47, 79, 83, 85, 101–106]. It is now realized that ordering is a structural property while fluidity is a dynamic concept. The detailed properties of probes such as orientation of the transition moments, cylindrical symmetry or not, fluorescence lifetimes and their temperature

variations have, however, not been taken fully into account. We believe these factors and the others discussed in detail to be important if proper characterization of lipid bilayers is to be achieved, and that the time is now ripe to use systematic theories of the type discussed in the previous section for proper data analysis.

There is, on the other hand, a large amount of data available which has given insight into membranes and which can help in planning future experiments. Here we wish to review briefly some of this work. We concentrate once more on the DPH probe, which we have used as an example and which is the most used. We look first at model membranes then at biological ones.

5.1. DPH in model membranes

As we discussed in §3, DPH has been widely studied as a highly sensitive fluorescent probe of membrane fluidity, because it exhibits a number of favourable structural and spectroscopic properties [79, 107]. In summary:

(a) Its high extinction coefficient and fluorescence quantum yield allow the detection of a fluorescence signal even at very low concentrations (e.g. 10^{-6} M).

(b) The well separated absorption and emission bands reduce the possibility of energy transfer between DPH molecules and facilitate the elimination of excitation light scattering.

(c) DPH is chemically stable and, being strongly lipophilic, is practically insoluble in water, while it is easily incorporated into membranes.

(d) Its rod-like shape causes it to align normally with the long axis parallel to the lipid chains.

(e) Absorption and emission moments are approximatively parallel to each other and to the long axis of the molecule, allowing the use of a simple formalism in the interpretation of the experimental data. Moreover this configuration of transition moments means high values of fluorescence polarization anisotropy in the ordered phase, which is particularly useful when trying to locate a phase transition e.g. in a membrane bilayer system.

It should be remembered, however, that DPH also shows some properties which require care when performing experiments as well as in the interpretation of the results:

(a) DPH partitions with a ratio one to one in the gel and liquid crystal phase of the lipids [102]. This behaviour is useful in the correct detection of the lipid transition temperature, but it implies that DPH can only give some average value of the membrane properties in the presence of more or less heterogeneous regions in the bilayer.

(b) The emission maxima of DPH are relatively insensitive to the type of solvent used, thus ruling out the possibility of using it as a polarity probe.

The absorption spectra are on the other hand sensitive to the solvent polarity. These spectra must however be used with care, owing to the difficulty of performing reliable absorption measurements in scattering media such as membranes.

(c) The possibilities of some photochemical reactions involving DPH, such as *cis-trans* isomerization or reactions with the solvent have been mentioned: e.g. Shinitzky and Barenholz [79] reported a reversible decrease of the DPH fluorescence in liposomes with the time of exposure to a light source. Birch and Imhof [81] have also found a new absorption band appearing in polar solvents at high energies. Furthermore DPH oxidation or the formation of a covalent complex between DPH and a lipid oxidation product has been reported [108] for the probe embedded in multilamellar vesicles containing egg phosphatidylcholine. These counter-indications have prompted a number of workers to investigate various DPH derivatives as potential fluorescent probes with improved features [107, 108].

A problem of particular relevance when using fluorescent probes in membranes is that of knowing the probe location in the bilayer, e.g. if it sits in the hydrophilic region near to the polar heads, or if it is more or less deeply buried in the hydrocarbon region. It is also very useful to know the likely orientation of the probe with respect to the lipid chains. Observing that the absorption spectrum of DPH in bilayers is similar to that in apolar organic solvents, and considering the insolubility of DPH in water, many authors [11, 102, 103, 110] agree that DPH is located in the hydrocarbon region of the bilayer. Owing to the rod-like structure of DPH and by analogy with oriented liquid crystals studies [67], the orientation of the DPH long axis in membranes is believed to be parallel to that of the lipid chains [9b, 111]. The time-dependent emission properties of DPH are thought to reflect roughly the average molecular motion of the hydrocarbon chains around DPH itself. The absorption spectrum of DPH does not change going from the liquid crystal to the gel phase [102]. This suggests that DPH sits in the apolar region of the membrane at the temperatures studied.

The theory discussed in the previous chapters relating fluorescence anisotropies to order parameters and correlation functions assumes depolarization to be caused by the probe reorientation. On the other hand depolarization by radiative or non-radiative energy transfer or excimer formation can occur at high probe concentrations. In order to avoid energy transfer, a lipid-probe molar ratio of at least 10^3 has been recommended [9b]. The analysis of the emission spectrum at probe concentration as high as 10^{-4} M in cyclohexane does not show any evidence of excimer formation.

Since DPH is insoluble in water and only fluoresces when absorbed inside the lipid bilayer its incorporation in membranes can be followed by measuring the increase of the fluorescence intensity with time [102]. The uptake of DPH by multilamellar liposomes is a more complex process than uptake by

small vesicles. In multilamellar systems the fluorescence intensity is found in fact to increase in a stepwise fashion [102]. This behaviour seems to indicate that DPH penetrates the multi-layered structure of liposomes and not just the outer layer.

The fluorescence lifetimes of DPH in various phospholipids bilayers range between 7.5 and 11 ns, depending on the temperature. They are approximately constant in the gel phase region and decrease with temperature in the liquid-crystal phase. We have seen in §3 that in apolar isotropic hydrocarbon solvents, e.g. mineral oil or liquid paraffin, the DPH fluorescence lifetime does not change with temperature, while it changes in polar hydrocarbon solvents as glycerin or propylene glycol. This suggests that the fluorescence lifetime of DPH depends both on the temperature and the polarity of the medium. Unfortunately the lack of absorption spectroscopic studies and of quantum yields data precludes the determination of the radiative lifetimes of DPH in model membranes and the comparison with data in organic solvents is difficult. It is interesting to note that DPH in saturated fatty acids has, at the same temperature, higher fluorescence lifetime values than in unsaturated ones. If polarity effects in the various fatty acids are negligible, one may hypothesize that the higher order in saturated fatty acids increases DPH fluorescence lifetime.

It has been reported [10, 112] that the decay of the total fluorescence intensity of the DPH in vesicle systems cannot be adequately described as a single exponential. The existence of two different sites in the membrane interior, or a reversible excited state reaction have been invoked to explain these data [10]. Chen et al. [10] also report that the fluorescence anisotropy decay is not monoexponential and attribute this to the lack of cylindrical symmetry for DPH. It might be worth re-examining this problem using a theory like the one given in §4.

The role played by cholesterol in membranes has been studied for many years using a variety of spectroscopic techniques [113–115]. In particular the effect of cholesterol on fluorescence parameters of DPH in membrane lipids has been investigated by a number of authors [9c, 12, 13, 29, 116]. Cholesterol is found to increase the order in the liquid-crystalline phase and to decrease it in the gel phase. In contrast the molecular dynamics seem to be almost unaffected. At high cholesterol concentrations (30–50%) the phase transition becomes practically unobservable. The lifetime of DPH decreases in the gel phase and increases in the liquid-crystalline phase in the presence of cholesterol. This fact indicates that DPH experiences different environments in the two phases after cholesterol addition. The behaviour of the fluorescence lifetime is very similar to that of the order parameter and supports the hypothesis that the order may influence DPH fluorescence lifetime. Johnson [117] has empirically found a linear relation between lifetime and polarization for DPH in liposome or cell membranes. Other

substances can, in principle, affect the fluorescence parameters of DPH in membranes. They include proteins and glycerides. Of particular interest is triolein, which does not affect the ability of cholesterol to suppress the phase transition, but drastically reduces the fluorescence polarization values [116, 117]. It is not clear, however, whether the order or the dynamics are affected since time-dependent measurements have not been performed.

5.2. DPH in biological membranes

A knowledge of the ordering and motional properties of molecules constituting biological membranes is important for an understanding of the mechanism of various membrane functions as well as of the modifications occurring in pathological transformations. In the previous sections we have pointed out the importance of the local orientational anisotropy of membranes in interpreting the fluorescence polarization properties of dissolved probes. In biological membranes another fact to be taken into account is that they have a heterogeneous structure and a complex biochemical composition, which includes different kinds of phospholipids, neutral lipids such as cholesterol, glycolipids and proteins. It is obvious that if anisotropy differences are found between normal and tumour cell membranes they should be correlated with differences in biochemical composition. For this purpose the precise location of the probe and the effect of each component on the probe fluorescence ought to be known to limit the possibility of misinterpretation. As an example DPH has been widely used in fluorescence anisotropy studies of whole cells, assuming that it penetrates only in the external plasma membranes. On the other hand Pagano et al. [118] have shown, using an autoradiographic method, that DPH, when incubated with intact lymphocytes or fibroplasts, locates itself not only inside the cell surface membrane, but also in the cytoplasmic and nuclear regions of the cell. It seems that DPH is principally located in the external membrane only in erythrocytes. Bouchy et al. [119] have recently analyzed the evolution of DPH fluorescence polarization following incubation in living cells. They found a decrease of both r_s and r_∞ with the incubation time, a decrease that is not present in isolated plasma membranes. They point out that the fluorescence parameters of DPH are characteristic of the plasma membranes at the start of the incubation period. At long times, however, most of the fluorescence signal is due to DPH embedded in intracellular lipids which are in a more fluid state than membrane lipids. It has also been suggested [120, 121] that non-membrane lipid droplets, which may occur in the cell cytoplasm, have a lowering effect on the apparent order parameters of intact cells. These findings raise serious doubts about the validity of using probes as DPH with intact cells, and suggest the convenience of working with isolated membranes in such studies.

Another point to take into account in membrane fluorescence studies, is that we are dealing with aqueous suspensions which scatter light, possibly with an attendant depolarization depending on the nature of the investigated biological material [122]. A theoretical treatment of light scattering depolarization has been given by Teale [123]. From a practical point of view it is convenient to correct for the induced light scattering depolarization by plotting r_s as a function of the sample absorbance at the probe emission wavelength. The true value of r_s is recovered by extrapolating to zero absorbance [117, 119, 122].

The spectroscopic properties of DPH in biological membranes are influenced by their composition. Studies in protein-membrane model systems have shown that DPH fluorescence polarization varies as the amount of protein in the bilayer changes, probably following order variations in the membrane. This is in accord with microcalorimetric and ESR techniques [124, 125]. Mely-Goubert and Freedman [126], however, suggest that the high fluorescence polarization values of DPH in membranes might reflect to a large extent interactions of the probe with proteins from the inner portions of the cell. This position is in contrast with that of van Blitterswijk et al. [120] who found no differences in polarization comparing isolated native membranes with liposomes prepared from their lipid extracts. An exception seems to be the human eye lens fibre membranes where they report an appreciable protein contribution to the order parameters. Other authors report a positive effect of proteins on DPH fluorescence polarization [127, 128]. This different behaviour may possibly depend on the type of membrane, on the type and concentration of proteins, and also on the position of the proteins in the bilayer. For instance Herreman et al. [128] has found that the pH dependence of fluorescence polarization of DPH in DMPC vesicles labelled with α-lactalbumin was related to the ability of the protein to penetrate the bilayer at acidic pH. In order to obtain a positive contribution of the proteins to fluorescence anisotropy, the probe should be assumed to partition into highly structurally ordered regions of the lipid, surrounding the apolar parts of membrane intrinsic proteins unless the probe interacts directly with proteins. This fact is known to be true in model lipid membranes [124]. The scattering of results in biological membranes, however, suggests that more studies are needed in order to clarify the question of the effect of proteins on DPH fluorescence polarization.

As mentioned earlier, the cholesterol effect on the fluorescence polarization of DPH has been widely studied in model membranes [9c, 12, 13] both in the gel and in the liquid crystalline phase. At room temperature biological membranes are normally in the liquid-crystalline phase and the effect of cholesterol is that of increasing the order of the membranes. In particular Kinosita et al. [130] have explained the greater order in erythrocyte mem-

branes with respect to sarcoplasmic reticulum membrane in terms of the higher cholesterol content, as evidenced by the difference in the values of the cone angle appearing in their model. The order parameter has also been found to be directly related to the cholesterol content in a variety of membranes from normal and tumour cells. Steady-state measurements also show dramatic changes in fluorescence polarization of DPH inside the lipid region of membranes belonging to normal and malignant cells. In particular in leukaemic cell membranes a decrease in polarization has always been found [131–133] on going from normal to lymphoma cells. It has been suggested that the factor mainly determining these differences could be a significant decrease in the molar ratio of cholesterol to phospholipids of the leukaemic cells. These facts have suggested that fluorescence polarization measurements could have a diagnostic and/or prognostic value [134]. The validity of this has on the other hand been questioned by Johnson [117] by investigating isolated plasma membranes. She found no difference between the cholesterol-phospholipid ratio in normal and lymphoma cells, and advanced the hypothesis that the differences in the DPH fluorescence parameters could be due to a variation of the glycerides in the plasma membrane. It is interesting to note that in solid tumours fluorescence polarization of DPH presents an opposite trend. In fact polarization and order increase going from normal to tumour cell membrane [93, 116, 117, 120, 135].

The problem of quantitatively describing order and fluidity in biological membranes is obviously of great interest, both from a fundamental and a practical point of view [129]. The best way of obtaining this information seems to be through time-dependent studies [130]. However the steady state technique is still very widely used because of its simplicity and it is worth investigating its information content in a real experimental situation. A simple relationship has been proposed by Heyn [14] and Jähnig [15] linking r_s to $\langle P_2 \rangle$ for DPH in lipid vesicles. The relation is obtained employing a strong collision-like expression for r_s (cf. Eqn. 4.94) assuming a ratio of fluorescence to reorientational decay time $\tau_F/\tau_0 \sim 8$, constant over the temperature range considered. While this might be plausible in relatively fluid lipid systems it is harder to justify, and generally incorrect, for biological membranes. An empirical relation linking r_s to $\langle P_2 \rangle$ for DPH has been put forward by van Blitterswijk et al. [120]. The equation proposed might be useful as a rough guide but it is hard to justify theoretically, at least in applications to systems where the $\langle P_2 \rangle$ variation is due to T variation. A tentative justification has been suggested based on the diffusion model examined earlier [120]. There are, however, some problems with this, due to the fact that the diffusion model predicts the polarization anisotropy decay to be given by a sum of exponentials, rather than just one as in the strong

collision-like models. Moreover the rotational diffusion coefficient itself varies with temperature and this variation should somehow be taken into account.

It should be stressed that proper analysis of continuous illumination data is not straightforward in view of the number of unknown parameters involved. To overcome this problem, we have developed a technique for the analysis of the steady state polarization anisotropy ratio r_s. This technique has been applied in the investigation of cell membranes obtained from normal and tumour cells with different growth rate, using DPH as fluorescent probe [93]. According to the theory developed in §4.3.3 the steady state polarization anisotropy for a rod-like molecule with transition moments parallel to the long axis is

$$r_s = r_0 \sum_K \sum_q (b^{q0})_K / [1 + (\alpha_{q0})_K D_\perp \tau_F] \qquad q = 0, \pm 1, \pm 2 \qquad K = 1, 2, 3 \ldots \tag{5.1}$$

where $D_\perp$ is the component of the probe diffusion tensor perpendicular to the long axis. It tells us how easy it is to reorient the long axis. τ_F is the fluorescence lifetime if we assume the fluorescence decay to be effectively mono-exponential. We recall from the previous sections that the coefficients $(b^{q0})_K$, $(\alpha_{q0})_K$ are obtained from the solution of the diffusion Eqn. 2.36. They are functions of the order parameter $\langle P_2 \rangle$ and can be calculated and tabulated once and for all, given a certain potential. The theory predicts the orientational correlation functions to be a sum of exponentials. In practice we have retained the first five exponentials (labelled by K) which result from a numerical solution of the diffusion equation according to the Nordio et al. theory [50]. The input parameters needed to predict r_s at a certain temperature are τ_F, $D_\perp$ and $\langle P_2 \rangle$. Thus even if we are only interested in extracting $\langle P_2 \rangle$ we have the problem of having more unknown than experimental data since $D_\perp$, τ_F and $\langle P_2 \rangle$ vary with temperature. To remedy this situation we have first of all measured τ_F at a series of temperatures. The intensity decays were found to be bi-exponential. For the sake of simplicity the suggestion of Kinosita et al. [130] of assuming an effective average decay time was followed. Then we have assumed a simple functional form for the variation of both $D_\perp$ and $\langle P_2 \rangle$ with temperature. Thus we assume

$$D_\perp(T) = (D_\perp)_{T_1} \exp\left[-E_R\left(\frac{1}{T} - \frac{1}{T_1}\right)\right] \tag{5.2}$$

i.e. an Arrhenius-type dependence, where T_1 is the highest experimental temperature for a certain series and E_R a rotational activation energy. We assumed moreover a quadratic dependence of $\langle P_2 \rangle$ on T, i.e.

TABLE 5.1
BEST FITTED VALUES FOR THE TEMPERATURE VARIATION OF $\langle P_2 \rangle$ AND $D_\perp$ AS FROM EQNS. 5.2, 5.3 [93]

Sample	T_1(°C)	$\langle P_2 \rangle_{T_1}$	$a \times 10^2$(°C^{-1})	$b \times 10^4$(°C^{-2})	$(D_\perp)_{T_1}$(ns^{-1})	E_R(kcal/mol)
Normal	52.0	0.074	0.42	0.26	0.13	5.4 ± 1
9618A	51.4	0.120	0.36	1.59	0.10	4.2 ± 1
H44	53.0	0.224	0.53	1.10	0.10	3.1 ± 1
H3924A	52.2	0.488	0.22	0.42	0.11	4.6 ± 1

$$\langle P_2 \rangle_T = \langle P_2 \rangle_{T_1} + a(T_1 - T) + b(T_1 - T)^2 \tag{5.3}$$

In biological membranes, as contrasted with pure lipid vesicles, the gel to liquid crystal transition is not normally observable [98]. The order parameter variation is thus assumed to be a smooth one [38]. With our assumption we try to mimick $\langle P_2 \rangle$ vs. T above the virtual gel to liquid crystal transition. Other functional forms for the $\langle P_2 \rangle$ vs. T curve can obviously be used in other situations.

In any case, use of Eqns. 5.2 and 5.3 allows us to analyze a given set of r_s vs. T results using a limited number of parameters which we optimize via a non-linear least squares fitting computer program. In particular we have examined microsomal membranes from rat liver, Morris hepatomas 3924A (fast growing), 44 (slow growing) and 9618A (very slow growing). Our results for the parameters involved in the fitting are given in Table 5.1.

The differences found in fluorescence polarization of DPH in normal and malignant cell membranes can provide, in our opinion, some insight in tumour investigation, provided that experimental data are properly analyzed and that variations in membrane composition are taken in due account.

Acknowledgments

We are grateful to C.N.R. (Rome) for supporting this work. A.A. thanks Federtrasporti for a A. Girandola Fellowship.

Appendix: Irreducible tensors and Wigner rotation matrices

A tensor of rank n is a quantity that transforms under rotation as the nth direct power of a vector. The 3^n dimensional representation of the rotation group realized in this way can be decomposed into a set of irreducible representations $D^{(L)}$ each of dimension $(2L + 1)$. The matrix elements of the

irreducible representation on a basis where the angular momentum operator J^2 and its projection J_z are diagonal with eigenstates $|Lm\rangle$, can be written as as

$$D^L_{m,n}(\alpha\beta\gamma) = \langle Lm|e^{-i\alpha J_z} e^{-i\beta J_y} e^{-i\gamma J_z}|Ln\rangle \tag{A1}$$

where α, β, γ are Euler angles defined according to the convention of Rose [25]. The matrix elements $D^L_{m,n}(\alpha\beta\gamma)$ are called Wigner rotation matrices, Wigner functions or generalized spherical harmonics. Combinations of ordinary tensor components transforming according to the representation $\boldsymbol{D}^{(L)}$ are called irreducible tensor components of rank L and denoted by $T^{(L,m)}$, e.g.

$$T^{(L,m)\gamma} = \sum_n D^L_{n,m}(\alpha\beta\gamma) T^{(L,n)} \tag{A2a}$$

$$T^{(L,m)} = \sum_n D^L_{m,n}(\alpha\beta\gamma)^* T^{(L,n)\gamma} \tag{A2b}$$

where the primed components refer to the rotated frame.

We have previously considered spherical irreducible tensors obtained from a second rank tensor **A** direct product of two equal vectors i.e. $\mathbf{A} = \boldsymbol{\mu} \otimes \boldsymbol{\mu}$. Let us consider the slightly more general case of a tensor $\mathbf{T} = \mathbf{a} \otimes \mathbf{b}$ i.e. the direct product of two possibly different vectors. The explicit irreducible components of **T** are given in Table A1. Equation A2 illustrates the main reason for the usefulness of irreducible tensors in problems involving rotations, i.e. that their transformation properties are very simple. The set of $(2L+1)$ components, $\mathbf{T}^{(L)}$, is called an irreducible tensor of rank L. From Eqn. A1 it is apparent that we can express $D^L_{m,n}(\alpha\beta\gamma)$ as

$$D^L_{m,n}(\alpha\beta\gamma) = e^{-im\alpha} d^L_{m,n}(\beta) e^{-in\gamma} \tag{A3}$$

TABLE A1

IRREDUCIBLE SPHERICAL COMPONENTS $T^{L,m}$ OF THE TENSOR $\boldsymbol{T} = \boldsymbol{a} \otimes \boldsymbol{b}$ IN TERMS OF THE CARTESIAN COMPONENTS OF THE VECTORS $\boldsymbol{a}$, $\boldsymbol{b}$

$$T^{0,0} = -(a_x b_x + a_y b_y + a_z b_z)/3^{1/2}$$
$$T^{1,0} = -i(a_y b_x - a_x b_y)/2^{1/2}$$
$$T^{1,\pm 1} = a_z b_x - a_x b_z \pm i(a_z b_y - a_y b_z)/2$$
$$T^{2,0} = (2/3)^{1/2}\{a_z b_z - (a_x b_x + a_y b_y)/2\}$$
$$T^{2,\pm 1} = \mp\{a_x b_z + a_z b_x \pm i(a_y b_z + a_z b_y)\}/2$$
$$T^{2,\pm 2} = \{a_x b_x - a_y b_y \pm i(a_x b_y + a_y b_x)\}/2$$

The real quantities,

$$d^L_{m,n}(\beta) = \langle Lm|e^{-i\beta J_y}|Ln\rangle \tag{A4}$$

are called reduced or small Wigner matrices.

The functions $D^L_{m,n}(\alpha\beta\gamma)$ constitute a complete orthogonal set spanning the space of the angles α, β, γ. When one or two of the subscripts are zero the Wigner rotation matrices reduce respectively to spherical harmonics or Legendre polynomials.

$$D^L_{m,0}(\alpha\beta 0) = \{4\pi/(2L+1)\}^{1/2} Y^*_{L,m}(\beta\alpha) \tag{A5}$$

$$D^L_{0,0}(0\beta 0) = d^L_{0,0}(\beta) = P_L(\cos\beta) \tag{A6}$$

where $Y_{L,m}$ is a spherical harmonic and P_L a Legendre polynomial. Some of their properties, which we frequently use, are:

Orthogonality

$$\int_0^{2\pi} d\alpha \int_0^{\pi} \sin\beta\, d\beta \int_0^{2\pi} d\gamma D^{L^*}_{m,n}(\alpha\beta\gamma) D^{L'}_{m',n'}(\alpha\beta\gamma) = 8\pi^2 \delta_{m,m'}\delta_{n,n'}\delta_{L,L'}/(2L+1) \tag{A7}$$

We also have the special cases

$$\int_0^{2\pi} d\alpha \int_0^{\pi} \sin\beta\, d\beta\, Y_{Lm}(\alpha\beta) Y_{L'm'}(\alpha\beta)^* = \delta_{LL'}\delta_{mm'} \tag{A8}$$

and

$$\int_0^{\pi} d\beta \sin\beta\, P_L(\cos\beta) P_{L'}(\cos\beta) = 2\delta_{LL'}/(2L+1) \tag{A9}$$

Closure: this allows coupling two successive rotations $(\alpha_1\beta_1\gamma_1)$ and $(\alpha_2\beta_2\gamma_2)$ to give a total rotation of $(\alpha\beta\gamma)$ as

$$\sum_n D^L_{m,n}(\alpha_1\beta_1\gamma_1) D^L_{n,m'}(\alpha_2\beta_2\gamma_2) = D^L_{m,m'}(\alpha\beta\gamma) \tag{A10}$$

Symmetry

$$D^{L^*}_{m,n}(\alpha\beta\gamma) = (-)^{m-n} D^L_{-m,-n}(\alpha\beta\gamma) = D^L_{n,m}(-\gamma-\beta-\alpha) \tag{A11}$$

TABLE A2

EXPLICIT EXPRESSIONS FOR THE SMALL WIGNER MATRICES $d^L_{m,n}(\beta)$ OF RANK $L = 0, 2$

Here $c = \cos(\beta/2)$ and $s = \sin(\beta/2)$.

$L = 0$

$d^0_{0,0} = 1$

$L = 2$

$d^2_{2,2} = d^2_{-2,-2} = c^4$

$d^2_{2,1} = -d^2_{2,-1} = -d^2_{1,2} = -d^2_{-1,-2} = -2c^3 s$

$d^2_{2,0} = d^2_{-2,0} = d^2_{0,2} = d^2_{0,-2} = 6^{1/2}c^2 - 6^{1/2}c^4$

$d^2_{2,-1} = -d^2_{-2,1} = -d^2_{1,2} = d^2_{1,-2} = -2s^3 c$

$d^2_{2,-2} = d^2_{-2,2} = s^4$

$d^2_{1,1} = d^2_{-1,-1} = -3c^2 + 4c^4$

$d^2_{1,0} = -d^2_{-1,0} = -d^2_{0,1} = d^2_{0,-1} = 6^{1/2}cs - 2(6^{1/2})c^3 s$

$d^2_{1,-1} = d^2_{-1,1} = 3s^2 - 4s^4$

$d^2_{0,0} = 1 - 6c^2 + 6c^4$

Products: the product of two Wigner rotations of rank L' and L'' with the same argument can be rewritten as a linear combination of Wigner rotation matrices of rank L according to the relation

$$D^{L'}_{m',n'} D^{L''}_{m'',n''} = \sum_{L=|L'-L''|}^{L'+L''} C(L'L''L; m'm'') C(L'L''L; n'n'') D^L_{m'+m'',n'+n''} \tag{A12}$$

where $C(abc; de)$ is a Clebsch-Gordan coefficient [25].

Integral of three Wigner rotation matrices: coupling two Wigner rotations as in Eqn. A12 and using the orthogonality relation Eqn. A7, the following useful integral can be obtained

$$\int d\alpha \sin\beta \, d\beta \, d\gamma \, D^{L''*}_{m'',n''}(\alpha\beta\gamma) D_{m',n'}(\alpha\beta\gamma) D^L_{m,n}(\alpha\beta\gamma)$$

$$= 8\pi^2 \delta_{m+m',m''} \delta_{n+m',m''} C(LL'L''; mm') C(LL'L''; nn')/(2L'' + 1) \tag{A13}$$

We now give the explicit expressions for the Wigner rotation matrices (and implicitly the order parameters i.e. their orientational averages). From Eqn. A3 we see that what we really need are expressions for the small matrices $d^L_{m,n}(\beta)$. In Table A2 we give explicit expressions for the most important cases $L = 0, 2$.

References

1 F. Perrin, J. Phys. Radium, Paris, 7 (1936) 1.

2 T.J. Chuang and K.B. Eisenthal, J. Chem. Phys., 57 (1972) 5094.

3 G.R. Fleming, A.E.W. Knight, J.M. Morris, R.J. Robbins and G.W. Robinson, Chem. Phys. Lett., 49 (1977) 1.
4 C. Zannoni, Mol. Phys., 38 (1979) 1813.
5 E.D. Cehelnik, R.B. Cundall, J.R. Lockwood and T.F. Palmer, J. Chem. Soc., Faraday Trans. 2, 70 (1974) 244.
6a I. Penchev and I. Dozov, Phys. Lett., A 60 (1977) 34.
6b I. Dozov and I. Penchev, J. Lumin., 22 (1980) 69.
7a T. Tao, Biopolymers, 8 (1969) 609.
7b G.K. Radda, Biomembranes, 3 (1972) 247.
8 G. Weber, in: A.A. Thaer and M. Sernetz (Eds.), Fluorescence Techniques in Cell Biology, Springer, New York, 1973.
9a K. Kinosita Jr., S. Kawato and A. Ikegami, Biophys. J., 20 (1977) 289.
9b S. Kawato, K. Kinosita Jr. and A. Ikegami, Biochemistry, 16 (1977) 2319.
9c S. Kawato, K. Kinosita Jr. and A. Ikegami, Biochemistry, 17 (1978) 5026.
10a L.A. Chen, R.E. Dale, S. Roth and L. Brand, J. Biol. Chem., 252 (1977) 2163.
10b R.E. Dale, L.A. Chen and L. Brand, J. Biol. Chem., 252 (1977) 7500.
11 M.P. Andrich and J.M. Vanderkooi, Biochemistry, 15 (1976) 1257.
12 W.R. Veatch and L. Stryer, J. Mol. Biol., 117 (1977) 1109.
13 K. Hildenbrand and C. Nicolau, Biochim. Biophys. Acta, 553 (1979) 365.
14 M.P. Heyn, FEBS Lett., 108 (1979) 359.
15 F. Jähnig, Proc. Natl. Acad. Sci. U.S.A., 76 (1979) 6361.
16a J.R. Lakowicz, F.G. Prendergast and D. Hogen, Biochemistry, 18 (1979) 508.
16b J.R. Lakowicz and J.R. Knutson, Biochemistry, 19 (1980) 905.
16c J.R. Lakowicz, H. Cherek, and D.R. Bevan, J. Biol. Chem., 255 (1980) 4403.
16d J.R. Lakowicz and G. Weber, Biophys. J., 32 (1980) 591.
16e J.R. Lakowicz, J. Biochem. Biophys. Methods, 2 (1980) 91.
17 G. Lipari and A. Szabo, Biophys. J., 30 (1980) 489.
18 R. Rigler and P. Grasselli, in: F. Hillenkamp, R. Pratesi and C.A. Sacchi (Eds.), Lasers in Biology and Medicine, Plenum Publ. Corp., New York, 1980.
19 C. Zannoni, Mol. Phys., 42 (1981) 1303.
20 J. Seelig, in: L.J. Berliner (Ed.), Spin Labeling: Theory and Applications, Academic Press, London, 1976.
21 B. Cannon, C.F. Polnaszek, K.W. Butler, L.E.G. Eriksson and I.C.P. Smith, Arch. Biochem. Biophys., 167 (1975) 505.
22 C. Zannoni, G.F. Pedulli, L. Masotti and A. Spisni, J. Magn. Reson., 43 (1981) 141.
23 C. Zannoni, in: G.R. Luckhurst and G.W. Gray (Eds.), The Molecular Physics of Liquid Crystals, chap. 3, Academic Press, London, 1979.
24 G.S. Beddard and M.A. West (Eds.), Fluorescent Probes, Academic Press, London, 1981.
25 M.E. Rose, Elementary Theory of Angular Momentum, Wiley, New York, 1957.
26 C. Zannoni and M. Guerra, Mol. Phys., 44 (1981) 849.
27 M. Abramowitz and I.A. Segun (Eds.), Handbook of Mathematical Functions, Dover, New York, 1964.
28 J. Suurkuusk, B.R. Lentz, Y. Barenholz, R.L. Biltonen and T.E. Thompson, Biochemistry, 15 (1976) 1393.
29 B. Lennart, A. Johansson and G. Lindblom, Q. Rev. Biophys., 13 (1980) 63.
30a K. Razi-Naqvi, Biophys. J., (1980) (preprint).
30b K. Razi-Naqvi, J. Chem. Phys., 74 (1981) 2658.
31a G.R. Luckhurst, in: G.R. Luckhurst and G.W. Gray (Eds.), The Molecular Physics of Liquid Crystals, chap. 7, Academic Press, London, 1979.
31b R.L. Humphries, P.G. James and G.R. Luckhurst, Symp. Faraday Soc., 5 (1971) 107.
32 G.R. Luckhurst, C. Zannoni, P.L. Nordio and U. Segre, Mol. Phys., 30 (1975) 1345.
33 L. Landau and E.M. Lifshitz, Statistical Physics, 2nd edn., Pergamon Press, Oxford, 1969.

34 G.R. Luckhurst and M. Setaka, Mol. Cryst. Liq. Cryst., 19 (1973) 279.
35a W. Maier and A. Saupe, Z. Naturforsch., A, 13 (1958) 564.
35b W. Maier and A. Saupe, Z. Naturforsch., A, 14 (1959) 882.
35c W. Maier and A. Saupe, Z. Naturforsch., A, 15 (1960) 287.
36 G.R. Luckhurst and C. Zannoni, Nature, 267 (1977) 412.
37 S. Marcelja, Biochim. Biophys. Acta, 367 (1974) 165.
38 F. Jähnig, J. Chem. Phys., 70 (1979) 3279 and refs. therein.
39 F.W. Wiegel and A.J. Kox, Adv. Chem. Phys., 41 (1980) 195.
40 G.R. Luckhurst, M. Setaka and C. Zannoni, Mol. Phys., 28 (1974) 49.
41 J. Seelig, Biochemistry, 13 (1974) 4839.
42 J.W. Emsley and J.C. Lyndon, N.M.R. Spectroscopy using Liquid Crystalline Solvents, Pergamon Press, Oxford, 1975.
43 C. Zannoni, Ph.D. Thesis, University of Southampton, 1975.
44 D. Wallach, J. Chem. Phys., 47 (1967) 5258.
45 E. Dubois-Violette, F. Geny, L. Monnerie and O. Parodi, J. Chim. Physique, 66 (1969) 1865.
46 R.J. Wittebort and A. Szabo, J. Chem. Phys., 69 (1978) 1722.
47 P. Wahl, M. Kasai, J.P. Changeux and J.C. Auchet, Eur. J. Biochem., 18 (1971) 332.
48 R.A. Mendelson, M.F. Morales and J. Botts, Biochemistry, 12 (1973) 2250.
49 K. Kinosita Jr., S. Kawato, A. Ikegami, S. Yoshida and Y. Orii, Biochim. Biophys. Acta, 647 (1981) 7.
50 P.L. Nordio and U. Segre, in: G.R. Luckhurst and G.W. Gray (Eds.), The Molecular Physics of Liquid Crystals, chap. 18, Academic Press, London, 1979.
51 See e.g. J. Boiden Pedersen, in: L.T. Muus and P.W. Atkins (Eds.), Electron Spin Relaxation in Liquids, chap. 2, Plenum, New York, 1972.
52 N. Wax (Ed.), Selected Papers on Noise and Stochastic Processes, Dover, New York, 1954.
53 G.R. Luckhurst and A. Sanson, Mol. Phys., 24 (1972) 1297.
54 B.J. Berne and R. Pecora, Dynamic Light Scattering, Wiley, New York, 1976.
55a P.L. Nordio, G. Rigatti, U. Segre, J. Chem. Phys., 56 (1972) 2117.
55b G. Agostini, P.L. Nordio, G. Rigatti and U. Segre, Atti Accad. Naz. Lincei Sez. 2, 13 (1975) 1.
56 C. Hu and R. Zwanzig, J. Chem. Phys., 60 (1974) 4354.
57 S. Chandrasekhar, Liquid Crystals, Cambridge University Press, Cambridge, 1977.
58 P.L. Nordio and U. Segre, Chem. Phys., 11 (1975) 57.
59 J. Yguerabide and M.C. Foster, in: E. Grell (Ed.), Membrane Spectroscopy, Springer Verlag, New York, 1981.
60 R.F. Chen and H. Edelhoch, Biochemical Fluorescence: Concepts, Vols. 1,2 M. Dekker, New York, 1975.
61 I.B. Berlman, Handbook of Fluorescence Spectra of Aromatic Molecules, Academic Press, London, 1971.
62 R.B. Cundall and A. Gilbert, Photochemistry, Nelson, London, 1970.
63 A. Kearwell and F. Wilkinson, in: G.M. Burnett and A.M. North (Eds.), Transfer and Storage of Energy by Molecules, Vol. 1, Wiley, New York, 1969.
64 R.G. Gordon, J. Chem. Phys., 45 (1966) 1643.
65 D.S. Urch, Orbitals and Symmetry, Penguin Books, London, 1970.
66 P. Soleillet, Ann. Phys., 12 (1929) 23.
67 E.D. Cehelnik, R.B. Cundall, C.J. Timmons and R.M. Bowley, Proc. R. Soc. London, Ser. A, 335 (1973) 387.
68 E.D. Cehelnik, R.B. Cundall, J.R. Lockwood and T.F. Palmer, Chem. Phys. Lett., 27 (1974) 586; J. Phys. Chem., 79 (1975) 1369.
69 B. Hudson and B. Kohler, Ann. Rev. Phys. Chem., 25 (1974) 437.

70 J.B. Birks and D.J.S. Birch, Chem. Phys. Lett., 31 (1975) 608.
71 J.B. Birks, G.N.R. Tripathi and M.D. Lumb, Chem. Phys., 33 (1978) 185.
72 T.C. Felder, K.J. Choi and M.R. Topp, Chem. Phys., 64 (1982) 175.
73 P.C. Alford and T.F. Palmer, Chem. Phys. Lett., 86 (1982) 248.
74 D.J.S. Birch and R.E. Imhof, Chem. Phys. Lett., 88 (1982) 243.
75 J.B. Birks, Photophysics of Aromatic Molecules, Wiley, New York, 1970.
76 S.J. Strickler and R.A. Berg, J. Chem. Phys., 37 (1962) 814.
77 R.C. Weast (Ed.), Handbook of Chemistry and Physics, 57th edn., The Chemical Rubber Company Press, Cleveland, 1976.
78 Landolt-Bornstein, Zehlenwerte und Funktionen, Band II Teil 5 and Teil 6, Springer Verlag, Berlin, 1970.
79 M. Shinitzky and Y. Barenholz, J. Biol. Chem., 249 (1974) 2652.
80 K. Schulten and M. Karplus, Chem. Phys. Lett., 14 (1972) 305.
81 D.J.S. Birch and R.E. Imhof, J. Phys. E, 10 (1977) 1044.
82 P.E. Zinsli, Chem. Phys., 20 (1977) 299.
83 V. Cogan, M. Shinitzky, G. Weber and T. Nishida, Biochemistry, 12 (1973) 521.
84 M.D. Barkley, A.A. Kowalczyk and L. Brand, J. Chem. Phys., 75 (1981) 3581.
85 M. Shinitzky, A.C. Dianoux, C. Gitler and G. Weber, Biochemistry, 10 (1971) 2106.
86 M.D. Barkley, A.A. Kowalczyk and L. Brand, in: R.H. Sarma (Ed.), Proc. Second SUNYA Conversation in the Discipline Biomolecular Stereodynamics, Vol. 1, Adenine Press, New York, 1981.
87 H. Rubsamen, P. Barald and T. Podleski, Biochim. Biophys. Acta, 455 (1976) 767.
88 W.R. Ware and B.A. Baldwin, J. Chem. Phys., 40 (1964) 1703.
89 W.R. Ware, J. Phys. Chem., 66 (1962) 455.
90a W.H. Melhuish, J. Phys. Chem., 65 (1961) 229.
90b W.W. Mantulin and G. Weber, J. Chem. Phys., 66 (1977) 4092.
91 C. Zannoni, C. Stremmenos, A. Vecli, A. Arcioni, D. Ruozi and L. Masotti, VII International Biophysics Congress and III Pan-American Biochemistry Congress Abstracts I.U.P.A.B., 1981, p. 60.
92 R.P.H. Kooyman, Y.K. Levine and B.W. van der Meer, Phys., 60 (1981) 317.
93 L. Masotti, P. Cavatorta, G. Sartor, E. Casali, A. Arcioni, C. Zannoni, G. Bartoli and T. Galeotti, in: T. Galeotti et al. (Eds.), Membranes in Tumour Growth, Elsevier/North-Holland, New York, 1982.
94 S. Sakagami, A. Takase, M. Nakamizo and H. Kakiyama, Bull. Chem. Soc. Jpn., 46 (1976) 2062.
95 W.L. Hubbel and H.M. McConnell, Proc. Natl. Acad. Sci. U.S.A., 64 (1969) 20.
96 H. Strubbe, Comput. Phys. Commun., 8 (1974) 1; ibid. 18 (1979) 1.
97 Y.K. Levine, Prog. Biophys. Mol. Biol., 24 (1972) 3.
98 G. Lenaz, G. Curatola and L. Masotti, J. Bioenerg., 7 (1975) 223.
99 A. Azzi, Methods Enzymol., 32 (1974) 234.
100 S.G. Carr, S.K. Khoo, G.R. Luckhurst and C. Zannoni, Mol. Cryst. Liq. Cryst., 35 (1976) 7.
101 R.A. Badley, W.G. Martin and H. Schneider, Biochemistry, 12 (1973) 268.
102 B.R. Lentz, Y. Barenholz and T.E. Thompson, Biochemistry, 15 (1976) 4521.
103 B.R. Lentz, Y. Barenholz and T.E. Thompson, Biochemistry, 15 (1976) 4529.
104 G.W. Stubbs, B.J. Litman and Y. Barenholz, Biochemistry, 15 (1976) 2766.
105a J.H. Fendler, Acc. Chem. Res., 13 (1980) 7.
105b G.D. Correll, R.N. Cheser III, F. Nome and J.H. Fendler, J. Am. Chem. Soc., 100 (1978) 1254.
106 M. Shinitzky and Y. Barenholz, Biochim. Biophys. Acta, 515 (1978) 367.
107 R.H. Bisby, R.B. Cundall, L. Davenport, I.D. Johnson and E.W. Thomas, in: G.S. Beddard and M.A. West (Eds.), Fluorescent Probes, Academic Press, London, 1981.

108 D.A. Barrow and B.R. Lentz, Biochim. Biophys. Acta, 645 (1981) 17.
109 F.G. Prendergast, R.P. Haugland and P.J. Callahan, Biochemistry, 20 (1981) 7333.
110 C. Sené, D. Genest, A. Obrenovitch, P. Wahl and M. Monsigny, FEBS Lett., 88 (1978) 181.
111 K.R. Thulborn, in: G.S. Beddard and M.A. West (Eds.), Fluorescent Probes, Academic Press, London, 1981.
112 C.D. Stubbs, T. Kouyama, K. Kinosita and A. Ikegami, Biochemistry, 20 (1981) 4257.
113 H.H. Mantsch, H. Saito and I.C.P. Smith, in: J.W. Emsley, J. Feeney, and L.H. Sutcliffe (Eds.) Progress in Nuclear Magnetic Resonance Spectroscopy, Vol. 11, Pergamon Press, Oxford, 1977.
114 I.C.P. Smith and K.W. Butler, in: L.J. Berliner (Ed.), Spin Labeling Theory and Applications, Academic Press, New York, 1976.
115 D. Chapman, R.M. Williams and B.D. Ladbrooke, Chem. Phys. Lipids, 1 (1967) 445.
116 R.P. van Hoeven, W.J. van Blitterswijk and P. Emmelot, Biochim. Biophys. Acta, 551 (1979) 44.
117 S.M. Johnson, in: G.S. Beddard and M.A. West (Eds.), Fluorescent Probes, Academic Press, London, 1981.
118 R.E. Pagano, K. Ozato and J.M. Ruysschaert, Biochim. Biophys. Acta, 465 (1977) 661.
119 M. Bouchy, M. Donner and J.C. André, Exp. Cell Res., 133 (1981) 39.
120 W.J. van Blitterswijk, R.P. van Hoeven and B.W. van der Meer, Biochim. Biophys. Acta, 644 (1981) 323.
121 E. McVey, J. Yguerabide, D.C. Hanson and W.R. Clark, Biochim. Biophys. Acta, 642 (1981) 106.
122 S.M. Johnson and C. Nicolau, Biochem. Biophys. Res. Commun., 76 (1977) 869.
123 F.W.J. Teale, Photochem. Photobiol., 10 (1969) 363.
124 D. Chapman, J.C. Gomez-Fernandez and F.M. Goñi, FEBS Lett., 98 (1979) 211.
125 J.C. Gomez-Fernandez, F.M. Goñi, D. Bach, C. Restall and D. Chapman, FEBS Lett., 98 (1979) 224.
126 B. Mely-Goubert and M.H. Freedman, Biochim. Biophys. Acta, 601 (1980) 315.
127 M. Rosseneu, R. Vercaemst, H. Caster, M.J. Lievens, P. van Tornout and P.N. Herbert, Eur. J. Biochem., 96 (1979) 357.
128 W. Herreman, P. van Tornout, F.H. van Cauwelaert and I. Hanssens, Biochim. Biophys. Acta, 640 (1981) 419.
129 L. Cercek, B. Cercek and C.H. Ockey, Biophys. J., 23 (1978) 395.
130 K. Kinosita Jr., R. Kataoka, Y. Kimura, O. Gotoh and A. Ikegami, Biochemistry, 20 (1981) 4270.
131 M. Inbar, M. Shinitzky and L. Sachs, FEBS Lett., 38 (1974) 268.
132 M. Shinitzky and M. Inbar, J. Mol. Biol., 85 (1974) 603.
133 M. Shinitzky and M. Inbar, Biochim. Biophys. Acta, 433 (1976) 133.
134 C. Jasmin, Y. Augery, F. Calvo, N. Larnicol, C. Rosenfeld, G. Mathe' and M. Inbar, Biomedicine, 34 (1981) 23.
135 M. Inbar, M. Shinitzky and L. Sachs, J. Mol. Biol., 81 (1973) 245.